Spring 1-1-2012

Predictive Modeling of Hydrogen Assisted Fatigue Crack Growth in Pipeline Steel

Neha Rustagi
University of Colorado at Boulder, neharustagi618@gmail.com

Predictive Modeling of Hydrogen Assisted Fatigue Crack Growth in Pipeline Steel

by

Neha Rustagi
B.S. University of Maryland, College Park, 2008

A thesis submitted to the
Faculty of the Graduate School of the
University of Colorado in partial fulfillment
of the requirements for the degree of
Master of Science
Department of Mechanical Engineering
2012

This thesis entitled:

Predictive Modeling of Hydrogen Assisted Fatigue Crack Growth in Pipeline Steel
Written by Neha Rustagi
has been approved for the Department of Mechanical Engineering

_____
Dr. Todd Murray

_____
Dr. Andrew J. Slifka

_____
Dr. Robert Amaro

Date_____

The final copy of this thesis has been examined by the signatories, and we find that both the content and the form meet acceptable presentation standards
of scholarly work in the above mentioned discipline.

Rustagi, Neha (M.S., Mechanical Engineering)

Predictive Modeling of Hydrogen Assisted Fatigue Crack Growth in Pipeline Steel

Thesis directed by Dr. Todd Murray

The growing government and industry interest in vehicles powered by hydrogen fuel cells has warranted research in recent years on use of the existing oil and natural gas pipeline infrastructure for widespread hydrogen fuel transport. Much of this research aims to assess the mechanical properties of pipeline steel in a hydrogen environment, as they are different from its properties in oil and natural gas. The current research analyzed the effects of 800 psi and 5000 psi environing hydrogen pressures on crack growth rates in acicular ferrite and ferrite pearlite steels when the steels were fatigued at frequencies of 1 Hz and 0.1 Hz at a load ratio of 0.5. A pressure of 800 psi was found to accelerate crack growth for the entirety of the Paris regime observed, and that of 5000 psi further accelerated crack growth in the beginning of the Paris regime. Crack growth rates were not influenced by variations in frequency and microstructure when the environing hydrogen pressure was 5000 psi, but they were faster in acicular ferrite than in ferrite pearlite in 800 psi of hydrogen. The experimentation was supplemented with finite element modeling of fatigue crack growth and stress-driven hydrogen diffusion in steel in ABAQUS. The modeling serves as a proof of concept, and can later be expanded to simulate hydrogen assisted fatigue crack growth. Such a full simulation would enable predictions of hydrogen assisted fatigue crack growth under given operating conditions, along with the derivation of new predictive relationships of hydrogen assisted crack growth based on parameters that are difficult to measure experimentally, such as plastic strain.

Acknowledgements

This work would not have been possible without the support of numerous others at the University of Colorado, Boulder and the National Institute of Standards and Technology (NIST).

I would like to thank my advisor, Dr. Todd Murray, other thesis committee members, Dr. Andrew J. Slifka and Dr. Robert Amaro, and other mentors at NIST, Dr. James R. Fekete and Ms. Elizabeth Drexler, for the tremendous amount of patience, guidance, encouragement and insights they provided, without which this research would not have been possible.

I would also like to thank other current and past members of my lab group at NIST who gave me support and experimental data without which this research would not have been possible. These members include Damian Lauria, Katie Eason, Brian Leach, April Stevenson, and Peter Keefe.

I would like to thank the University of Colorado, Boulder's Department of Civil Engineering for giving me access to an ABAQUS student license that enabled me to conduct finite element modeling for this research.

Finally, I would like to thank Mr. James Merritt at the U.S. Department of Transportation and the Professional Research Experience Program between NIST and the University of Colorado, Boulder for the financial support and research opportunity that made this thesis possible.

TABLE OF CONTENTS

List of Tables

List of Figures

1 Introduction

The use of the existing oil and natural gas pipeline infrastructure to transport hydrogen fuel is gaining research interest as hydrogen fuel cell vehicles gain significance to the U.S. government and automobile industry. Widespread use of hydrogen fuel cell vehicles will require a reliable mode of hydrogen transport, and the pipeline infrastructure is the most cost-effective, efficient means of nationwide hydrogen transport available today. Safe use of these pipelines in a hydrogen environment requires new codes and standards, however, regulating their operation and maintenance. Generation of these codes and standards necessitates more research on the behavior of steel in a hydrogen environment, as hydrogen has been known to influence the mechanical properties of pipeline steel differently than oil or natural gas. The extent of hydrogen-induced damage that is expected to manifest in any pipeline will determine the operating conditions in which the pipeline can be safely used to transport hydrogen, the frequency with which inspections should be conducted, and the extent of damage that should tolerated before a pipeline is taken out of service. Hydrogen-induced damage can take many forms, such as acceleration of crack growth, and the extent of damage is a function of many different variables, including the frequency of loading, hydrogen pressure, and steel microstructure. The multitude of these interrelated variables makes hydrogen's effects difficult to assess through analytical means, and therefore makes finite element modeling an attractive approach to predictions of hydrogen-assisted crack growth.

The current research aimed to:

- Analyze experimental data to assess the effects of pressure, frequency, and steel microstructure on hydrogen assisted fatigue crack growth rates in steel. These analyses can additionally be used in the future to calibrate finite element models of hydrogen-assisted fatigue crack growth.

- To demonstrate finite element modeling of fatigue crack growth and stress-driven hydrogen diffusion in pipeline steel as a proof of concept. The finite element model created in the current research can be expanded in the future to simulate hydrogen assisted fatigue crack growth. The full numerical simulation can then be used to make crack growth rate predictions in a variety of different loading conditions in hydrogen, and to derive new relationships between a steel's mechanical properties and hydrogen assisted crack growth rates in the steel. Such a simulation will have particular value in the generation of relationships between hydrogen-assisted crack growth rate and material properties that are difficult to assess analytically, such as crack tip plasticity. Crack tip plasticity is commonly negligible in cyclic loading, such that relationships based on linear elastic fracture mechanics can easily be used to predict crack growth rates. These relationships are invalid, however, when crack tip plasticity is significant, as it may be after an overloading event. In conditions of significant plasticity, predictive relationships between hydrogen assisted crack growth rate and the magnitude of crack tip plasticity may be of great value. Finite element modeling would aid not only in the derivation of these relationships, but also in determination of the magnitude of crack tip plasticity in given loading conditions.

2 Background

2.1 Fracture Mechanics of Steel

The linear elastic stress field within an annular region surrounding a crack tip is described by a parameter known as the stress intensity factor, K. Derivations of K can be found in the literature, and are based on the application of equations describing the stress field surrounding a sharp linear elastic crack to the crack tip itself. One of the common assumptions in these derivations is that the strain energy surrounding a crack is bounded at the crack tip. Given this assumption, at the crack tip, higher

order terms in the equations describing the stress field vanish, such that the stress field at the crack tip can be described exclusively by K, a parameter known as the 'T term', and measures of the far-field stresses. Real cracks are not perfectly sharp, however, and have a small plastic zone in front of them known as the process zone; the process zone causes the crack to blunt. (1) Derivations of K are frequently applied to annular zones surrounding blunt cracks, where the inner radius of the annulus is at the boundary of the process zone. Within this annulus, the higher order terms are commonly treated as negligible, and the stress field is approximated exclusively by K, the T-term, and the far-field stresses. The T-term becomes significant in short fatigue cracks, cracks "under mixed-mode loading where the in-plane shear stresses are substantially larger than the tensile stresses" (2), cracks in certain specimen geometries in plane strain, and "small cracks inclined at a small angle to the far-field tensile axis" (2). When none of these conditions apply, the T term is frequently negligible , however, and is thus omitted, such that the stress field in the annular region is described exclusively by K and the far-field stresses. (2)

The length of the outer radius of the aforementioned annular zone is dictated by the significance that the T term and higher order terms take on as distance from the crack tip increases; when it becomes unacceptably inaccurate to approximate the stress field by K alone, the other terms must be included. (2) Moreover, when the process zone in front of the crack tip is sufficiently small (as is commonly the case in fatigue), it is treated as negligible, such that K is used exclusively to describe the stress field surrounding the crack tip, even though the crack is blunt; "small scale yielding" (SSY) is the name given to this condition, whereby a blunt crack is approximated as being sharp and it is valid to neglect the higher order terms and the T-term. (3) If a material is being fatigued in SSY, the Paris Law is commonly used to predict crack growth behavior as a function of ΔK and empirical constants that are determined based on properties of the material itself, as well as the manner in which it is being loaded:

$$\mathbf{1} \quad \frac{da}{dN} = C\Delta K^m ,$$

where da/dN is the crack growth rate, C and m are empirical constants, and ΔK is the range of stress intensity factors the material will experience in the fatigue cycle. (2)

The above argument for using K exclusively to characterize the stress field in the linear elastic annular zone surrounding a crack tip (while ignoring the nonsingular and higher order terms) has been criticized because its derivation is based on the assumption that strain energy is bounded. While strain energy is bounded at the crack tip and within the process zone, it is not bounded in the surrounding annular zone where K is intended to be applied. An alternative derivation of the stress field at a crack tip in Mode III loading was proposed by (3), and can be expected to be similar for Modes I and II loading. In this derivation, the closed form solutions of tractions in the annular zone lead to the conclusion that the K term dominates all other nonsingular and higher order terms if and only if the following conditions is met:

$$\mathbf{2} \quad O\left(\frac{\rho}{\left(\frac{K_{III}^{A}}{\tau_a}\right)^2}\right) \ll 1\,,$$

where K_{III}^{A} is the stress intensity factor, ρ is the characteristic dimension of the plastic zone (such as its radius), and τ_a is the traction being applied to the specimen boundary (3).

This condition will be satisfied when the typical conditions of small-scale yielding are also satisfied. These conditions are:

$$\mathbf{3} \quad \left(\frac{\tau_a}{\tau_o}\right)^2 = C^{-1} * \frac{\rho}{R}$$

where τ_a is the traction being applied to the specimen boundary, τ_o is the inelastic traction at the outer boundary of the plastic zone, C is a first order constant, ρ is the characteristic dimension of the plastic zone, and R is the outer radius of the annular zone,

and

$$\rho/R << 1 \quad \textbf{4}$$

Therefore, even though strain energy is not bounded within the annular region surrounding the crack tip, as long as the typical conditions of small-scale yielding are satisfied, the K term will dominate all other terms in stress field within the annular zone. (3)

The advantage of using K to approximate a stress field is that it enables convenient predictions of crack growth, given basic information about a material's properties and the far-field stresses. However, this approximation can be invalid when the plasticity at a crack tip is significant and the conditions of SSY do not hold. For instance, if a material is subject to variable loading, an overload can result in the generation of a large process zone that may eventually retard crack growth by exerting "high residual compressive stresses" on the crack (4). Such conditions are common in dynamically loaded structures (4), and use of K to predict crack growth rate may be unacceptably inaccurate in these cases.

An alternative description of the local stress field surrounding a crack is Neuber's Rule. Neuber's Rule has three forms, each of which relate the local stress and strain at the crack tip to the far field stress and strain, while accounting for the process zone. The form of Neuber's Rule for nominally elastic behavior is:

$$\frac{(K_t S)^2}{E} = \sigma\epsilon, \quad \textbf{5}$$

Where K_t is the theoretical stress concentration factor as defined below, S is the applied load, E is the modulus of elasticity, σ is the local stress at the crack tip, and ε is the local strain at the crack tip.

$$K_t = \frac{\sigma_{max}}{S}, \quad \textbf{6}$$

where σ_{max} is the maximum local stress at the crack tip.

Approximations have been derived to relate Neuber's Rule to the traditional measure of stress intensity in cyclic loading, ΔK. One such approximation for a short crack is:

$$\mathbf{7} \quad \Delta K = 1.12 K_t \Delta S \sqrt{\pi l},$$

where l is the length of the crack.

Predictions of ΔK made using Equation 7 are likely to be inaccurate, however, because the process zone for short cracks is large; predictions of crack growth rate made using this value of ΔK are thus also likely to be inaccurate. Nevertheless, the existence of this approximation and the known relationships between K_t and ε, as defined by Neuber's Rule, and between ΔK and da/dN, as defined by the Paris Law, lends support to the hypothesis that a relationship exist between the local strain at a crack tip, ε, and crack growth rate, da/dN. One potential application of the finite element modeling component of the current research is to aid in the derivation of such a relationship for hydrogen embrittled steels.

2.2 Diffusion of Hydrogen into Steel

Hydrogen enters steel through normal interstitial lattice sites (NILS), and then diffuses toward regions of lower chemical potential to diminish the chemical potential gradient. Regions of lower chemical potential include those with higher tensile hydrostatic stress and softened elastic moduli; the former may result from the application of stress to the material (as in fatigue) (5), and the latter can be caused by hydrogen that enters the lattice (6). Hydrogen entering the lattice additionally exerts volumetric strain on the lattice, which, at high concentrations, can also have a small effect on the stress within the lattice. The microstructure of the steel also impacts diffusion, as the diffusivity of hydrogen is eight orders of magnitude greater in body-centered cubic (BCC) phases (such as α' martensite and

ferrite), than in face-centered cubic phases (such as austenite), and hydrogen is thus more likely to accumulate and develop critical concentrations requisite for damage in BCC steel. (7)

Diffusing hydrogen accumulates at microstructural heterogeneities that serve as traps; these include “dislocations, grain boundaries, inclusions, voids, surfaces and impurity atoms” (5). The populations of hydrogen in NILS and in trapping sites can be assumed to be in chemical and mechanical equilibrium as long as the rate at which traps are filled and depleted is faster than the rate at which a stressed region of the steel lattice relaxes, such that empty traps are always present during straining of the lattice; the NILS hydrogen reaches equilibrium with the local stresses when plastic straining and the creation of new traps stop. (5) Hydrogen assisted fracture is of particular concern at grain boundaries, as impurities and alloying elements, such as “Mn, Si, S and P”, segregate to boundaries and may attract additional hydrogen while causing decohesion themselves. (8) In some metals, hydrogen assisted fracture propagates primarily along grain boundaries (9) (8), which is of particular concern because intergranular cracking can occur at subcritical stresses, and thereby result in unexpected catastrophic failure (8).

The distribution of hydrogen around a notch or crack tip is therefore determined by two competing mechanisms: the generation of traps by plastic straining and the application of tensile hydrostatic stress. Trapped hydrogen accumulates near the surface of the crack tip, where the density of traps is greatest (since plasticity is greatest). NILS hydrogen accumulates a distance from the notch or crack surface, where triaxial stresses are greatest. In materials with low hydrogen solubility, such as steels, in small scale yielding, the strain rate determines the location of maximum hydrogen concentration (5). At rapid strain rates, hydrogen does not diffuse through NILS fast enough to fill the traps being generated in the highly plastic region. These traps are thus filled by the nearby NILS, which are consequently depleted. The concentration of hydrogen is therefore greatest in the plastic region.

At slow strain rates, new traps are generated slowly enough that diffusing hydrogen is able to fill them, such that hydrogen concentration is greatest in the region of high hydrostatic stress. The blunting of a crack tip often makes this strain rate effect negligible, as the hydrogen in trapping sites surrounding a blunt crack is much greater than that in the surrounding NILS. Alternatively, in materials with high hydrogen solubility, such as niobium, the density of trapping sites is relatively small, and the hydrogen concentration prior to straining determines whether hydrogen will accumulate at trapping sites or at regions of high stress. If the initial concentration is below a given threshold, the trapping mechanism is likely to dominate, and if the concentration is instead greater than the threshold, the hydrostatic stress dominates. (5) The distribution of hydrogen in a material can determine the kind of fracture the hydrogen causes- growth of a single crack, or initiation of multiple microcracks, indicative of environmental fatigue cracking. (10)

Another prominent theory on the manner in which hydrogen is transported into and within steel is that it is carried by mobile dislocations (7). This theory is currently unresolved (unlike the mechanisms of hydrostatic stress and trapping sites), but is a possible explanation for the speed of hydrogen transport through steel lattices, and is consistent with the fracture mechanisms observed in steel tensile specimens tested in hydrogen. According to the mechanism of dislocation transport, hydrogen adsorbs to the steel surface, dissociates, and then binds to dislocations located at or near the steel surface. The hydrogen atoms bound to a dislocation are then transported by the mobile dislocation. Even at ambient temperatures, “dislocations can carry hydrogen deep into a specimen” (11). Dislocations can lose their hydrogen clouds if they move too rapidly, are annihilated, or approach hydrogen traps or grain boundaries. If a mobile dislocation intersects a grain boundary it cannot traverse, such as a high angle grain boundary, the hydrogen clouds surrounding the dislocation will saturate the grain boundary and then rapidly transfer to any of the dislocations being generated in the adjacent grain. Alternatively, when a dislocation approaches an inclusion, any surrounding hydrogen is likely to escape from the

dislocation, as hydrogen has a greater affinity for inclusions than it does for dislocations. Any hydrogen that escapes a dislocation is likely to either diffuse through the steel lattice, or accumulate in a void, where it has been theorized to recombine to create H_2 and contribute to local fracture. Weakly bonded inclusions as small as 50 Angstroms are often nucleation sites for microvoids. Strongly bonded inclusions are less likely to nucleate voids, and hydrogen surrounding such inclusions is thus likely to contribute to fracture by weakening interfacial bonds, rather than building pressure within the voids as a result of hydrogen gas formation. Some of the hydrogen accumulating in a void will escape into the lattice, but the rate of hydrogen escape is significantly less than the rate at which voids are charged. Consequently, large hydrogen pressures may develop within voids and cause the voids to grow more rapidly than they would otherwise. Such accelerated microvoid growth is the manner in which steel being tensile tested in hydrogen was originally thought to fail. The validity of the theory of accelerated microvoid growth has, however, since been heavily debated. (11)

2.3 Mechanisms of Hydrogen Induced Damage

Several different theories have been proposed to date regarding the mechanism of hydrogen induced damage. One of the well understood and accepted causes of hydrogen induced damage is the introduction of hydrogen to a steel lattice in a manner that generates large gradients of hydrogen concentration at the steel's surface. Large gradients can generate "high stresses near the surface" (12), nucleate dislocations, and/or generate hydrides within the material, all of which have the potential to harden the material (13). Hydrides can also form if stress is applied to a metal that already contains hydrogen within its lattice. Hydrides embrittle materials by causing deformation that promotes slip, resulting in localization of dislocations and/or shear stresses. Localized slip and shear stresses may macroscopically increase the material's flow stress or reduce it, depending on the extent to which the hydrogen mobilizes dislocations. Shear localization may also occur if the distribution of hydrogen within

a material is inhomogeneous. (12) While hydrides may form in certain metals, they are not known to form in steels. As such, hydrogen is instead more likely to damage steels by a combination of several other mechanisms. Three of the most prominently studied mechanisms of hydrogen induced damage are: 1) hydrogen enhanced localized plasticity (HELP), 2) hydrogen induced dechoesion (HID), and 3) adsorption induced dislocation emission (AIDE). All three of these theories are described in detail below, and can be applied in conjunction with a fourth theory known as the Petch adsorption criterion. According to this criterion, hydrogen that adsorbs to a crack lowers the "surface-free energy of the crack surface" (14), and, since this energy contributes to the stress required to propagate the crack, the adsorbed hydrogen lowers the requisite stress (14) (15).

It is important to note that heterogeneities within steel can cause dramatic differences between the predicted and actual stress intensities at a crack tip. For instance, if a crack in steel is loaded to a given K and the K is subsequently lowered, the threshold hydrogen pressure required to propagate the crack at the lower K will be greater than it would have been if the initial loading had not taken place. This appears to be due to the plastic zone that is created by the initial loading, and that remains even when the stress intensity is lowered. The hydrogen pressure requisite for crack propagation at the lower K must account for compressive forces exerted by the surrounding plastic zone. (14) Residual stresses and prior deformation that generate plastic zones within a material will influence the stress intensity that develops at a crack tip, and must be accounted for in predictions of hydrogen assisted crack growth (and crack growth in general).

2.3.1 Hydrogen Induced Decohesion

According to the hydrogen induced decohesion (HID) theory, hydrogen causes fracture by weakening the bonds in a steel lattice, such that they eventually break at lower applied stresses than would be requisite in air (10) (14). Since hydrogen-induced fracture occurs rapidly, hydrogen

surrounding the “free surfaces being formed” (10) is unlikely to have time to reach equilibrium with the surrounding “stress and strain fields” (10), and the concentration at the tip of a growing crack is thus likely to be much greater than it would be at equilibrium. (10) Moreover, crack fronts are theorized to have regions in which non-Hookean elastic stresses become large enough that they significantly lower the dissolved hydrogen’s chemical potential. This lower potential drives additional diffusion, such that the hydrogen concentrations that develop in these regions are ultimately several orders of magnitude greater than they would be at equilibrium. (14) The HID theory was once thought to be supported by experimentation showing that a stationary crack in a wedge open loaded (WOL) specimen being firmly held in place in a hydrogen chamber can be induced to propagate solely by increasing the hydrogen pressure; it was originally thought that such propagation could not occur due to any mechanism that depends on dislocation mobility, but the validity of this claim has since been argued. This experimentation moreover demonstrated the existence of a clear inverse relationship between the threshold hydrogen pressure at which a stationary crack will propagate and the stress intensity being applied to the crack; this relationship suggests that, above a given threshold, hydrogen reduces the cohesive strength between the atomic bonds in a steel lattice enough that they break. (14) HID is also supported by analyses showing that fracture in the presence of hydrogen frequently occurs without significant local deformation (12).

2.3.2 Hydrogen Enhanced Localized Plasticity

The hydrogen-enhanced localized plasticity (HELP) theory suggests that hydrogen embrittles materials by increasing the mobility of dislocations and thereby reducing the local flow stress in given regions of the steel to an extent that is proportional to the local hydrogen concentration (12). These regions of localized plasticity limit macroscopic ductility, thereby embrittling the material everywhere else (5). At low strain rates and temperatures wherein the hydrogen solutes are highly mobile,

hydrogen mobilizes dislocations by shielding them from the forces exerted by neighboring dislocations, regardless of their signs, and thereby enables a more fluid mobility (12). The effect appears to be independent of the steel's crystal structure or the type of dislocation (13). At extremely high concentrations, hydrogen may even make a repulsive stress field between dislocations attractive instead, resulting in the "coalescence of leading dislocations at the head of a pile-up and the formation of a crack" (12). HELP is supported by fractography showing plastic deformation in the fracture surfaces of hydrogen embrittled metals (12) (13), and by the presence of a greater number and greater spatial distribution of slip steps on steel surfaces indented in hydrogen as opposed to air (6); the change in slip step distribution indicates that dislocations are gliding at lower shear stresses than would be requisite in air.

Hydrogen shields dislocations by exerting volumetric strain on the material's lattice and by changing the material's constitutive moduli (12). TEM analyses of metal in hydrogen support the theory of dislocation shielding by showing that the addition of hydrogen to a metal lattice increases dislocation velocities and decreases the distances between dislocations themselves, as well as between dislocations and grain boundaries. Removing hydrogen gas from the metal's environment sometimes stops dislocation motion and other times additionally reverses it. One reason for the former effect may be that impurities in the crystal lattice sometimes pin dislocations in place when the hydrogen is removed. When hydrogen gas is reintroduced to the specimen, the dislocations start moving again, but a greater hydrogen pressure is now necessary to attain the same dislocation velocities attained initially. (13)

2.3.3 Adsorption Induced Dislocation Emission

An alternative treatment of the dimpling observed on the fracture surfaces of specimens exhibiting hydrogen induced damage is the adsorption induced dislocation emission (AIDE) theory. According to the AIDE mechanism, hydrogen adsorbed within "the first few atomic layers beneath the

surface" of a metal facilitates dislocation emission from a crack tip by lowering the stress required for dislocation nucleation (16). The premature nucleation of dislocations has been demonstrated in indentation simulations of nickel in hydrogen, and in indentation experimentation on stainless steel (17) (18). Large enough clusters of displaced atoms can form dislocation loops that grow until they form stable complex structures. Hydrogen appears not only to aid in dislocation nucleation, but also to cause these loops to emit dislocations at loads lower than would be requisite with air. Dislocations in hydrogen are moreover likely to be highly concentrated, and result in the generation of intense slip bands, since hydrogen enhances slip planarity. (18) Regions of dislocation concentration appear to enhance the formation of localized vacancies, which can lead to void formation and the nucleation of sharp cracks at much lower strains than would be required in inert environments (16) (18); the energy requisite for vacancy formation is additionally lowered by the mere presence of hydrogen in the lattices of many metals (18). As a crack in hydrogen grows, additional microvoids may form within the crack tip plastic zone, and are likely to interact "with the intense slip band" generated by dislocation emission and thereby maintain a sharp crack tip. (19)

Several different reasons have been hypothesized for the reduction hydrogen causes in the stress required for dislocation nucleation. One reason may be that hydrogen weakens interatomic bonds in the lattice (16), and another may be that hydrogen lowers the stacking fault energy of the lattice (17). Another reason may be that hydrogen softens the elastic moduli of steels. The shear stress required for dislocation nucleation has been shown to decrease in a hydrogen environment, while the ratio of this shear stress to the shear modulus of the material remains relatively constant; the consistency of this proportion indicates that the reduction in shear stress is likely due to the decrease in elastic modulus. (17) The influence of hydrogen on dislocation nucleation appears to be limited, however, to within "a few angstroms from the crack tip" (17).

The theory of AIDE was originally proposed as a mechanism for liquid metal embrittlement, which, like hydrogen embrittlement, results in localized slip, and, sometimes, dimpled fracture surfaces. Crack growth in liquid metal environments typically occurs too rapidly for chemical reactions that would embrittle the solid metal to occur; adsorption (rather than absorption) was thus hypothesized to be the primary phenomenon causing embrittlement. Upon discovery of the similarities between fracture surfaces of hydrogen embrittled steels and those of metals that had been embrittled by liquid metal, the theory was extended to hydrogen embrittlement. (16) The argument that near-surface adsorption must be dominant in hydrogen embrittlement has been called into question, however, by analyses "of H diffusion from the crack tip surface to damage sites in the FPZ." (19) Moreover, a large weakness in support for AIDE is that "the structure of slip" around a crack tip in a metal in hydrogen has not been "characterized sufficiently to show H stimulated dislocation emission and geometric crack extension" (19). Additionally, high strength polycrystalline alloys frequently contain significant "barriers to dislocation motion", such that AIDE may not be able to occur (19). AIDE also does not explain intergranular cracking that is frequently observed in embrittled materials (19).

2.3.4 Impact of Hydrogen on Slip Planarity

An alternative approach to analyzing hydrogen induced damage is the study of the impact hydrogen has on slip, as hydrogen has been shown to inhibit cross-slip and promote planar slip. The enhancement of planar slip is one way that hydrogen may promote fracture. Positive correlations between a steel's nitrogen content and its vulnerability to hydrogen assisted fracture have similarly been theorized to be due to the fact that nitrogen promotes planar slip. (7)

When mixed dislocations in steel cross-slip, the screw component of the dislocation must lengthen while the edge component shortens. In-situ microscopy of dislocation motion in high-purity Al has shown that a hydrogen atmosphere prevents such cross-slip by stabilizing the edge components of

dislocations. One reason for this effect may be that, in Al, the energy of the metal lattice in a hydrogen atmosphere is slightly lower if the hydrogen atmosphere is concentrated around an edge dislocation than if it is uniformly distributed or concentrated around a screw dislocation. Hydrogen is thus likely to concentrate around the edge components of mixed dislocations. If the edge converts to a screw component, some of the surrounding hydrogen will return to the steel lattice, and the entire system will have a greater energy configuration than it did originally. Since cross-slip of mixed dislocations requires edge components to convert to screw components, it is likely to be too energy-intensive to occur in Al, and perhaps in other metals as well. (20) The promotion of slip planarity by hydrogen environments is further bolstered by hardness tests that show that an indentation of steel is far more likely to cause two dislocations to nucleate (as opposed to just one) in hydrogen than in air. The nucleation of a second dislocation is hypothesized to be due to the inhibition of cross-slip, which makes a second dislocation nucleation excursion necessary for an indentation to continue. (6)

Hydrogen has additionally been shown to lower the stacking-fault energy (SFE) in metals (13). The separation distance between a pair of partial dislocations in a material is determined by a balance between the repulsive forces between them and the attractive forces the stacking fault exerts on them. The partial dislocations move in tandem to cross slip, and significant separation distances (due to low stacking fault energies) could therefore impede their cross slip. (21) The reduction in stacking fault energy due to hydrogen is often not high enough, however, to significantly impede cross-slip (13). Nevertheless, the reduction in SFE may additionally contribute to hydrogen assisted fracture by influencing dislocation transport of hydrogen. Since dislocations are less likely to cross slip at low SFEs, they are more likely to lose their hydrogen clouds when they reach inclusions, which may result in localized regions of damage (11).

2.4 Hydrogen Assisted Crack Growth Modeling

Several attempts have been made to date to quantitatively predict the effect of hydrogen on the stress required for void nucleation and/or crack growth in a matrix. One recent study integrated the HELP and HID mechanisms in a cohesive zone model. The study treated HELP by quantifying the localized stress reductions in a matrix due to high hydrogen concentrations, and treated HID by devising a traction separation law that relates the hydrogen-induced reduction in matrix cohesive strength to crack growth in the matrix. HID and HELP are similar in that both mechanisms decrease the flow stress required for crack growth, but are different in that the former also decreases the strain required for void nucleation while HELP increases it. This study assumed that hydrogen enters a matrix only through lattice diffusion, and did not account for dislocation transport. (10) Similarly, a traction separation law was devised in (22) that relates the tractions at a crack tip to hydrogen coverage around the crack. This law was then successfully implemented in the finite element modeling software ABAQUS to model fatigue crack growth in the presence of hydrogen. (22)

One goal of the current research was to model stress-assisted hydrogen diffusion in ABAQUS, such that a tractions separation law, such as the one in (22), could later be implemented and used to model hydrogen assisted fatigue crack growth in the steel. Such a model would enable assessment of plastic strains at the crack tip, as determined by ABAQUS, such that they could later be related to crack growth rate.

2.5 Impact of Microstructure on Hydrogen Diffusion and Damage

High strength steels are more susceptible to hydrogen induced damage than low strength steels. One reason for this may be that they typically have fewer sulphide inclusions than low strength steels. Such inclusions are hydrogen traps, and, the fewer there are, the greater the pressure around each inclusion; greater pressures may result in greater damage. (23) Moreover, “higher strength materials

can sustain higher hydrostatic tensile stresses than lower-strength materials, particularly at crack tips", and are consequently likely to be operated at higher stresses (8). The concentration of hydrogen that develops in a lattice as a function of hydrostatic tensile stress may be described by the following equation:

$$C_{La} = C_L e^{(\frac{\sigma_H V}{RT\sigma})}, \quad \textbf{8}$$

where C_{La} is the equilibrium lattice hydrogen concentration in the presence of hydrostatic tensile stress, C_L is the lattice hydrogen concentration in the absence of hydrostatic stress, σ_H is the hydrostatic tensile stress, V is the partial molar volume of hydrogen, R is the ideal gas law constant, and T is temperature. (8)

Greater concentrations of hydrogen are thus likely to develop in a steel being operated at higher stresses. Furthermore, the hydrogen concentration requisite to initiate or propagate intergranular fracture decreases as the stress in a material increases. Grain boundaries in steels being operated at higher stresses are thus more sensitive to any concentration of hydrogen. (8) Lower strength steels are additionally more likely to work harden than high strength steels. During cyclic loading, the fracture toughness of a low strength steel is thus more likely to increase than that of a high strength steel, such that it will become more resistant to crack growth regardless of its environment. (24)

The susceptibility of steel of a given grain size to hydrogen induced damage appears to increase as the microstructure changes from ferrite pearlite to martensite (23). The enhancement of damage susceptibility in martensite is likely due to the enhanced hydrogen diffusion rates in martensite, as discussed in Section 2.2. Tensile tests of hydrogen charged ferrite-pearlite steel show fracture to occur by cleavage in shallow dimples, known as rosettes. The rosettes typically have at least one inclusion at their centers, and failure around them occurs in a ductile or "mixed ductile-quasi-cleavage" (23) manner

manifested in ductile ridges. The dimples in uncharged ferrite-pearlite are deeper than these rosettes, and the failure more ductile. Fracture of bainitic steel is more brittle in both air and hydrogen than that of ferrite-pearlite steel. Tensile testing in uncharged specimens results in fracture surfaces with extensive ductile dimpling, while testing of charged specimens results in rosettes that are shallower than those in ferrite-pearlite steel. Fracture of charged martensitic steels is characterized by brittle cleavage at grain boundaries, such as triple points, with some ductile "microvoids between cleavage regions" (23); the density of dimples is lower than it is in ferrite-pearlite, and inclusions do not appear to play nearly as significant a role in fracture initiation. The greater the prior austenite grain size (23), the more susceptible martensite appears to be to hydrogen embrittlement. While the density of rosettes does often increase with grain size, the susceptibility of steel to embrittlement in uniaxial tension appears to depend much more strongly on microstructure than on grain size or yield strength (23) (7).

Increasing the concentration of nickel in hydrogen-precharged austenitic stainless steel reduces the steel's susceptibility to hydrogen damage. Nickel has this effect because it stabilizes austenite (thereby preventing it from transforming into martensite), and additionally raises the steel's stack fault energy. The effect of raising nickel content on ductility plateaus at a concentration of about 12%, at which point the positive correlation between nickel content and stacking fault energy also plateaus. Carbon also stabilizes austenite and raises the stacking fault energy of steel slightly, but its effect on hydrogen damage is much less than that of nickel. (7)

2.6 Effect of Loading on Hydrogen Induced Damage

The manner in which a material is loaded has a significant impact on hydrogen's ability to enter the material's lattice, and on its subsequent interactions with the lattice. In both cyclic and sustained loads, hydrogen can markedly decrease the fracture toughness of a material, such that cracks will initiate at lower stresses. Additionally, hydrogen can accelerate Stage II crack growth and promote

"premature Stage III crack growth" (9). At crack growth rates of about 10^{-5} mm/cycle or higher, hydrogen environments accelerate the Stage II growth of cracks being stressed above a given threshold crack tip stress intensity factor, K. The threshold value of K is termed K_{1SCC} in sustained loading, and K_{max}^{T} in cyclic loading (24), and the two values can differ in low strength steels. One reason for this difference is that cyclic loading makes all materials more susceptible to hydrogen damage because it continuously sharpens crack tips, thereby continuously exposing fresh metal to hydrogen. (24) This effect of cyclic loading is bolstered by experimentation showing that, at a constant Kmax, hydrogen increasingly accelerates crack growth as ΔK increases ($\Delta K=K_{max}-K_{min}$, where K_{min} is the minimum stress intensity applied to a crack during a fatigue cycle and K_{max} is the maximum stress intensity applied during the fatigue cycle, is a metric commonly used in fatigue crack growth relationships) (9). The frequency of cyclic loading and the pressure of the hydrogen environment can also influence hydrogen assisted crack growth, as, slower frequencies give hydrogen more time to enter the steel lattice and higher pressures make it more likely to do so (24). The hydrogen concentration that develops within a metal at equilibrium and the pressure of the environing hydrogen are frequently related with Sievert's Law (14) (17).

Crack closure phenomena may be significant enough at slow crack growth rates to have a large impact on the extent to which hydrogen accelerates crack growth. For instance, at crack growth rates below about 10^{-6} mm/cycle, hydrogen can accelerate crack growth at stress intensities below K_{max}^{T}. This acceleration appears to be due to crack closure phenomena that occur in air, but not in hydrogen. Air environments are frequently moist, unlike hydrogen environments, and oxides form on the surfaces of a crack as a result of the moisture. The plasticity-induced crack closure, and significant mode II shear displacements that manifest at near-threshold crack growth rates (regardless of environment) cause these oxides to develop into a thick film within the crack. The film thickens as the crack opens and closes, and the oxides can then significantly increase the amount of stress required to open the crack.

Such oxide-induced crack closure is exacerbated when load ratios (load ratio = K_{min}/K_{max}) are small and when the size of the crack tip opening approximates that of the oxides. (24) The effects of this layer on fracture can be seen in the fracture surfaces of materials fatigued in air. Fatigue in air typically results in "well-defined ductile striations", while fatigue in a vacuum instead results in far less regular, less continuous markings that give a "rumpled" appearance (16). The lack of distinctive striations in a vacuum is potentially due to the absence of the oxide film, which may prevent slip and crack tip blunting. (16)

Similarly, at a fixed ΔK, if the stress ratio is below a threshold value, the acceleration of crack growth by hydrogen appears to decrease with increasing stress ratio (rather than increase, as would be the case above the threshold.) (9) The reason for this decrease in acceleration may be that hydrogen reduces "the extent of plastic deformation at the crack tip" (25), such that crack tip plasticity does not decelerate crack growth (9) (25) as it would in air; the impact of plasticity induced closure can be expected to decrease in air as the stress ratio increases, while the impact in hydrogen can be expected to be negligible.

The failure mechanisms of tensile steel specimens in air (intergranular fracture "with occasional ductile tearing" (26), followed by transgranular cleavage and ductile tearing, and culminating with microvoid "nucleation, growth, and coalescence" (7)) typically also manifest in materials charged with hydrogen. Ductile failure is likely to be accelerated in hydrogen, however, and a larger number of microvoids can be expected to nucleate, most of which will be smaller than those seen in air. These mechanisms of ductile failure are additionally likely to be supplemented with secondary cracking in hydrogen atmospheres (26). The difference in microvoid distribution is consistent with the HID and HELP mechanisms, as HID predicts that hydrogen lowers the strength of atomic bonds in steel and HELP predicts that hydrogen additionally localizes slip bands, which impinge on particles (7) and thereby

generate higher interfacial stresses. This enhancement of stress in the material and simultaneous decrease in material strength may cause more, smaller microvoids to nucleate. (7) Materials with greater fracture stresses in hydrogen have been shown to also exhibit greater proportions of dimpled failure in hydrogen. (26)

The strain rate imposed on a material can also influence the impact hydrogen has on a material. At high strain rates, hydrogen atmospheres trail behind dislocations, rather than moving with them, and may actually impart enough drag force on them to reduce their mobility and macroscopically harden the material. (12) This phenomenon has been observed in hardness tests on stainless steel alloys, that show hydrogen lengthening dislocation multiplication excursions, most likely by slowing the dislocations down (6). This has also been seen in tensile tests of Ni_3Al specimens, in which hydrogen significantly reduces elongation until failure at slow strain rates but has only a negligible impact at high strain rates (26) (27).

2.7 Reducing Susceptibility of Steel to Hydrogen Induced Damage

Some research has been done to date on means of reducing the effects of hydrogen on steel. One method of reducing hydrogen induced damage is the addition of gases to the environment that are more likely to adsorb to the steel than hydrogen is. Oxygen, sulfur dioxide, and carbon monoxide, for instance, have all been shown to inhibit the acceleration of crack growth rate by hydrogen. Oxygen has additionally prevented Stage III crack growth from initiating prematurely, and carbon monoxide has additionally inhibited hydrogen-induced premature crack initiation. All of these effects likely occur because hydrogen is less likely to adsorb to the steel in the presence of these gases. At high concentrations, inhibitor gases may additionally displace adsorbed hydrogen. (9)

Alternatively, the engineering of “special” low energy grain boundaries has been shown to reduce a material’s susceptibility to premature intergranular fracture in hydrogen. Engineering of low-energy grain boundaries, “such as annealing twins and their variants”, into nickel alloys has been shown

to significantly increase fracture toughness, lengthen Stage II crack growth, and reduce the fraction of fracture that is intergranular in hydrogen environments of 2300-3900 appm (8). There are several potential reasons for these effects. The “special grain boundaries” may be stronger than random grain boundaries, and the critical hydrogen concentration they require for premature crack initiation may thus be greater. Alternatively, the “binding energy of hydrogen” to random grain boundaries may be greater than that to special grain boundaries, such that hydrogen is less likely to bind to (and subsequently weaken) special grain boundaries (8). These phenomena may be independent of the purity of the steel, as fractions of intergranular fracture have been shown to decrease even in the absence of sulphur inclusions at the intergranular fracture surfaces. (8) Research in the field of grain boundary engineering may shed light not only on ways of preventing hydrogen induced damage but also on the dominating mechanisms of hydrogen assisted crack growth.

3 Hydrogen Assisted Fatigue Crack Growth Experimentation

Data analysis of hydrogen assisted fatigue crack growth experiments performed at the hydrogen facility at the National Institute of Standards and Technology (NIST) in Boulder, CO was conducted as part of the current research. Compact tension (C(T)) specimens were fatigued using a 250 kN MTS servo-hydraulic load frame, and a 10-specimen load transfer system (Figure 1). The transfer system is composed of clevises that transfer load evenly to each of the specimens, and links that bypass the load on a specimen once the crack length reaches a preset limit.

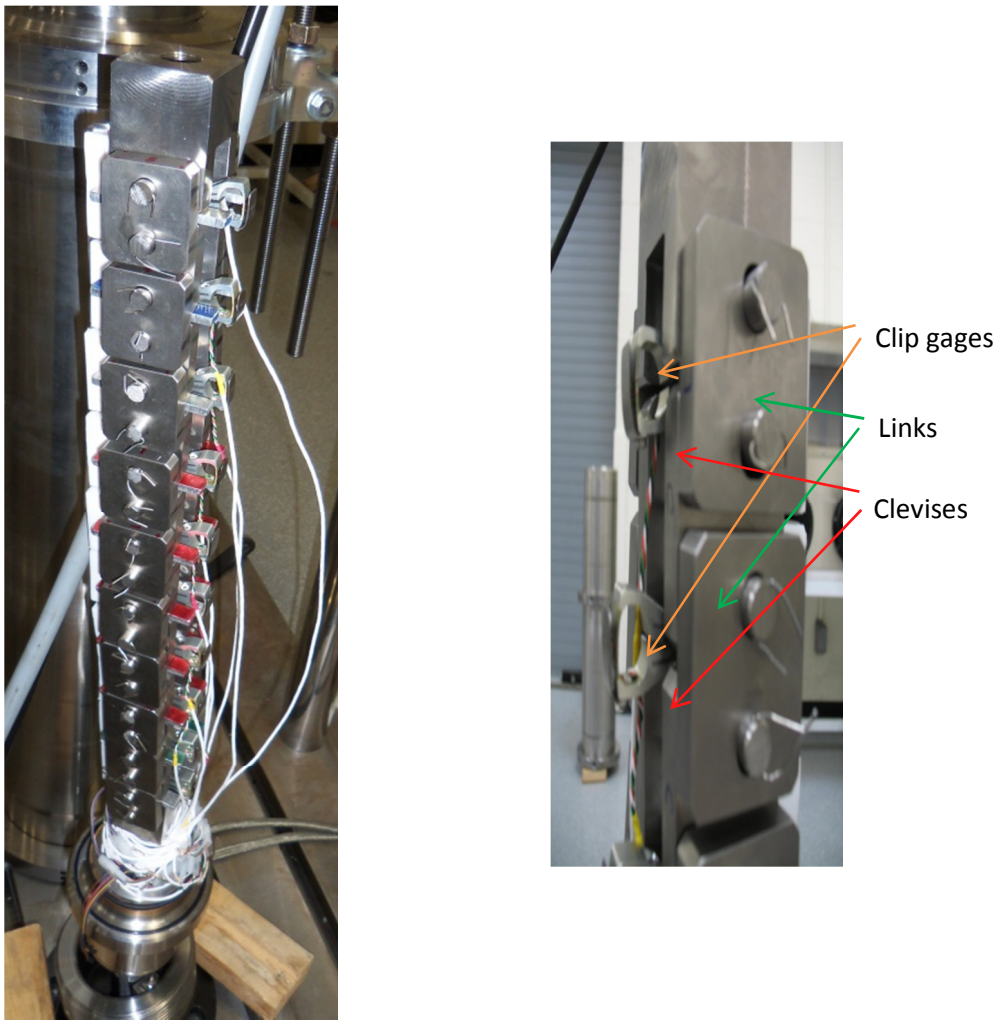

Figure 1 10-specimen load transfer system used to fatigue steel specimens

A LabView program was used to maintain the gas environment and operate the associated safety systems. The specimens were machined out of pipeline steel provided by two pipeline suppliers that will hereon be referred to as Suppliers A and B. The Supplier A steel is 2011 X52 acicular ferrite carbon steel, while the Supplier B steel is 1963 X52 ferrite-pearlite carbon steel. The chemical compositions of both steels are provided in Table 1 and

Table 2 below, and micrographs of both steels are provided in Figure 2 and Figure 3 below.

Table 1 Chemical Composition of Steel from Supplier A

Al	B	C	Co	Cr	Cu	Fe	H	Mn	Mo	N
0.002	<0.0001	0.238	0.004	0.014	0.085	98.48	0.0001	0.96	0.004	0.003
Nb	**Ni**	**P**	**S**	**Si**	**Ti**	**V**				
0.001	0.05	0.011	0.021	0.064	0.002	0.002				

Table 2 Chemical Composition of Steel from Supplier B

Al	B	C	Co	Cr	Cu	Fe	H	Mn	Mo	N
0.017	<0.0001	0.017	0.002	0.033	0.016	98.37	0.0006	1.06	0.003	0.004
Nb	**Ni**	**P**	**S**	**Si**	**Ti**	**V**				
0.026	0.016	0.012	0.004	0.24	0.038	0.004				

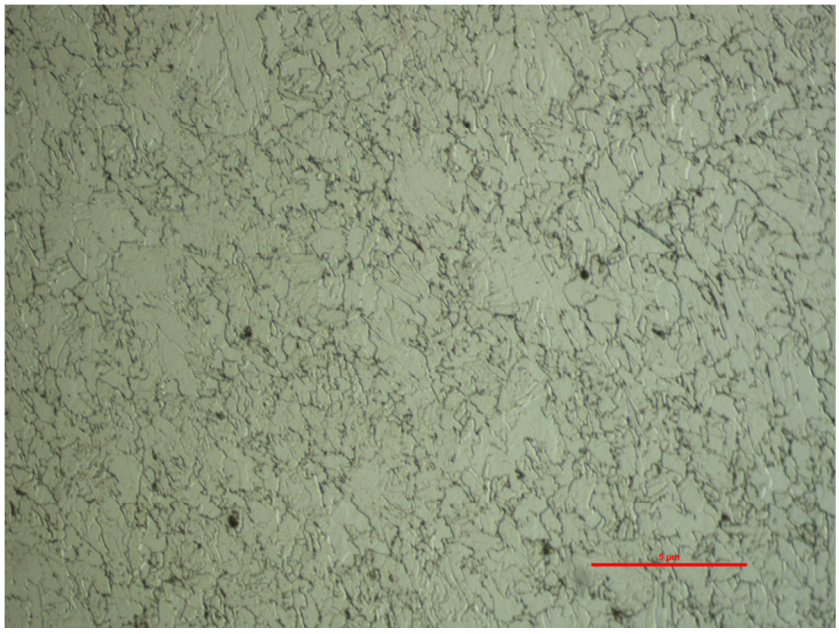

Figure 2 Optical Microstructure of Supplier A Steel

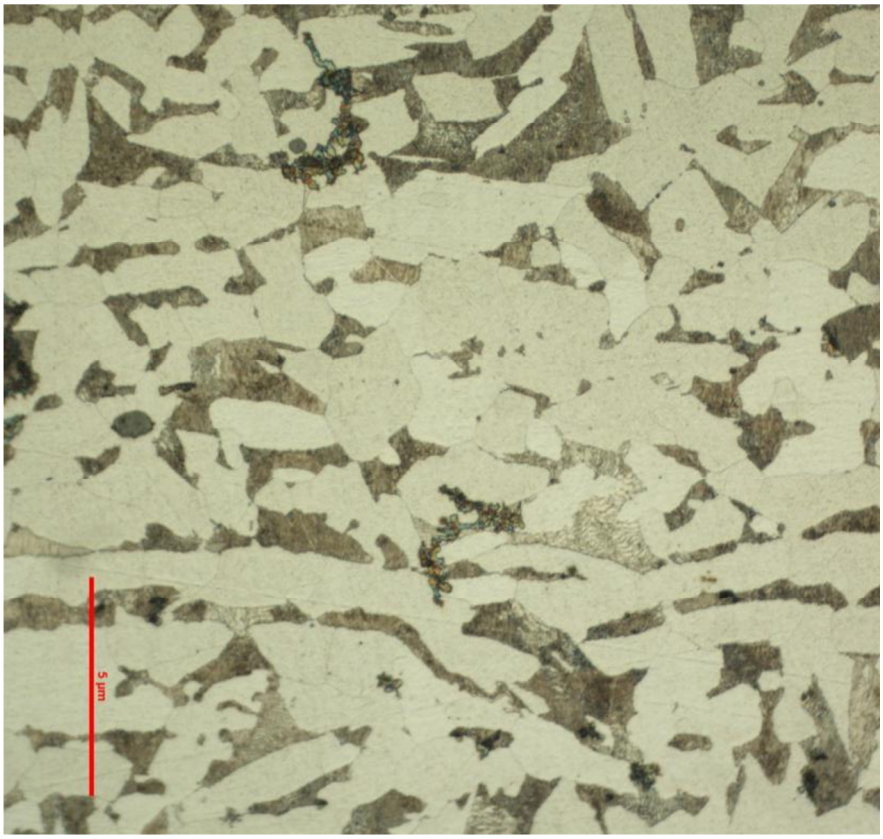

Figure 3 Optical Microstructure of Supplier B Steel

The roughness of the C(T) specimens was characterized with profilometry, and all specimens were brought to a standard roughness of <250 nm using a succession of sand paper and diamond slurry treatments as needed. Clip gauges with a resolution of 2 µm were used to measure the crack mouth opening displacement (CMOD) in each of the specimens.

CMOD values and the values of applied load were used to calculate crack lengths, crack tip stress intensity factor ranges (ΔK), and crack growth rates for each of the specimens, per ASTM Standard E647-05. These calculations were performed in a program written by the author in Wolfram Mathematica. ASTM Standard E647-05 requires that an effective modulus of elasticity be calculated for all specimens being analyzed. At the time of this thesis, effective moduli had not yet been determined for all of the specimens analyzed, and a modulus of 210 GPa was therefore used in all specimen analyses.

Sets of fatigue testing in four different environments and loading conditions were completed at a stress ratio (where stress ratio is defined as K_{min}/K_{max}) of 0.5. The test environments were: air at 1 Hz, 800 psi hydrogen at 1 Hz, 5000 psi hydrogen at 1 Hz, and 5000 psi hydrogen at 0.1 Hz.

3.1 Impact of Hydrogen Pressure

The concentration of hydrogen in the lattice sites of any metal at equilibrium is known to be a positive function of the square root of the environing hydrogen pressure (28). As would therefore be expected, many past studies have quantified a positive correlation between environing hydrogen pressure and the effects of hydrogen on a material's mechanical properties. Tensile testing has shown the percentage reduction of notch strength in metal alloys in a hydrogen environment to be linearly related to an exponential of hydrogen pressure (29)- the square root or less, and tensile testing and fatigue crack growth testing have both shown the percentage reduction of ductility to also be linearly related to the square root of environing hydrogen pressure (29) (30). A fracture criterion for metal alloys in hydrogen has additionally been derived based on a negative linear correlation between the environing hydrogen concentration and fracture strength (31). Moreover, the critical threshold stress intensity for crack growth has been shown to be linearly related to the logarithm of the environing hydrogen pressure (32).

As might be expected, crack growth acceleration may only be affected by hydrogen pressure when the pressure is varied within given upper and lower bounds; lowering the pressure below the lower bound or raising it above the upper bound has been shown to have no effect on crack growth rates (28) (31). The existence of a lower bound lends support to the hypothesis that a critical hydrogen concentration is requisite for hydrogen assisted cracking to occur within a given time frame (31). The existence of an upper bound lends support to the hypothesis that the hydrogen assisted cracking

mechanism depends predominantly on absorbed hydrogen (rather than adsorbed), and that the lattice sites surrounding a crack tip saturate at a given pressure (28).

Figure 4 and Figure 5 below compare the crack growth rates of steel specimens from each of the two aforementioned suppliers, A and B, at varying hydrogen pressures. In all specimens, a hydrogen pressure of 800 psi definitively accelerated crack growth, but raising the hydrogen pressure from 800 psi to 5000 psi had little effect on crack growth rates at high ΔK values toward the end of the Paris regime.

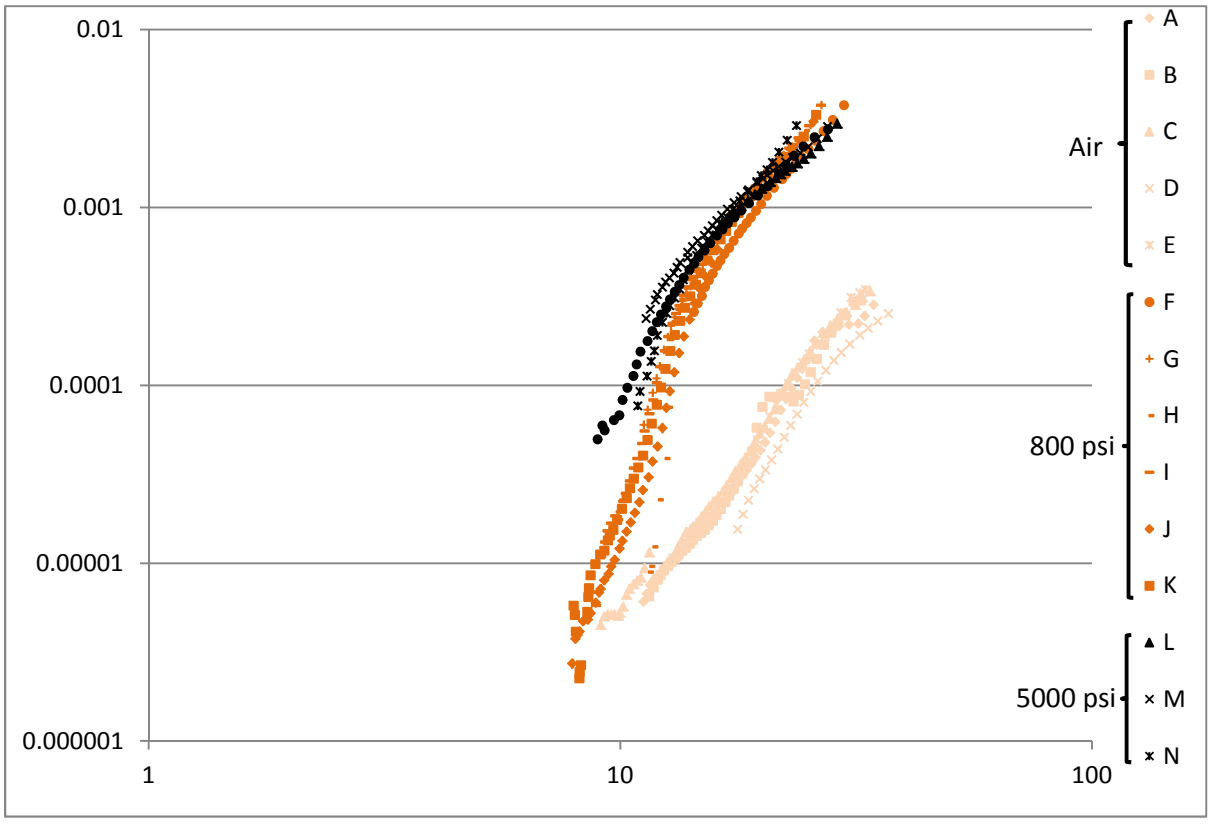

Figure 4 Specimens from Supplier A that were fatigued at 1 Hz at a stress ratio of 0.5 in air and at two different pressures. Specimens were arbitrarily labeled A-N.

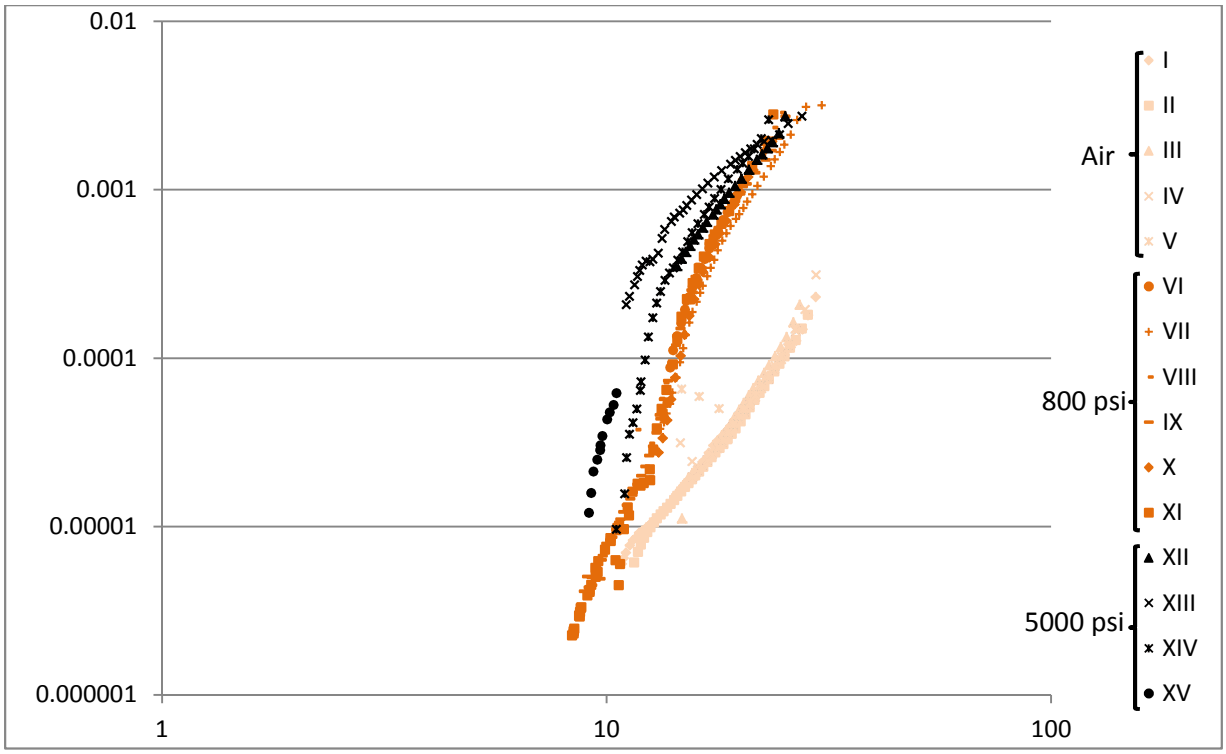

Figure 5 Specimens from Supplier B that were fatigued at 1 Hz at a stress ratio of 0.5 in air and at two different pressures. Specimens were arbitrarily labeled I-XV.

3.2 Impact of Loading Frequency

The frequency of loading applied to any steel in the hydrogen infrastructure depends on its application. Steels used inside hydrogen fuel cell vehicles will be subject to cyclic loading every time the vehicle is filled. (30) Pipeline steel undergoes cyclic loading due to "daily pressure fluctuations" and shutdowns and startups. (9) The interplay between the cyclic load frequency and crack growth rate can significantly impact a steel's susceptibility to hydrogen assisted crack growth. Results from experimentation can not be used to accurately predict crack growth rates in real-world applications if the experimentation is conducted at loading frequencies significantly different from those applied in practice, unless relationships are derived between crack growth rates at different frequencies.

Crack growth rates in hydrogen can be expected to be much higher at lower load frequencies, as lower frequencies give environing hydrogen more time to diffuse to the crack tip (33) and additionally

result in less strain hardening, which decelerates crack growth in all environments (7). Lower frequencies of loading have also been shown to accelerate crack growth rates in water vapor environments, wherein lower frequencies give hydrogen in the water vapor more time to dissociate on specimen surfaces and then enter the specimen lattices. (34) (35) The acceleration of hydrogen-assisted crack growth by lowering of loading frequency is, however, expected to plateau at sufficiently low frequencies wherein the amount of hydrogen that is able to diffuse to a traversing crack tip also plateaus. (35) (30) At near-threshold crack growth rates, the effect of frequency on crack growth has been shown to diminish even in vacuum, due to the diminishing magnitude of strain hardening in the near-threshold regime (7). The effect of frequency on crack growth in hydrogen also diminishes at low load ratios, wherein the crack is open for a lesser portion of the loading cycle (potentially due to the influence of crack closure at lower loads) and the ability of hydrogen to enter the lattice is thus significantly diminished at all loading frequencies. (34)

Figure 6 and Figure 7 below compare the effects of loading frequency on crack growth as measured in the current research. Two frequencies- 0.1 Hz and 1 Hz- were applied in 5000 psi of hydrogen to steel specimens from the two different aforementioned suppliers. Varying the frequency did not appear to have a significant effect on crack growth rates in these specimens.

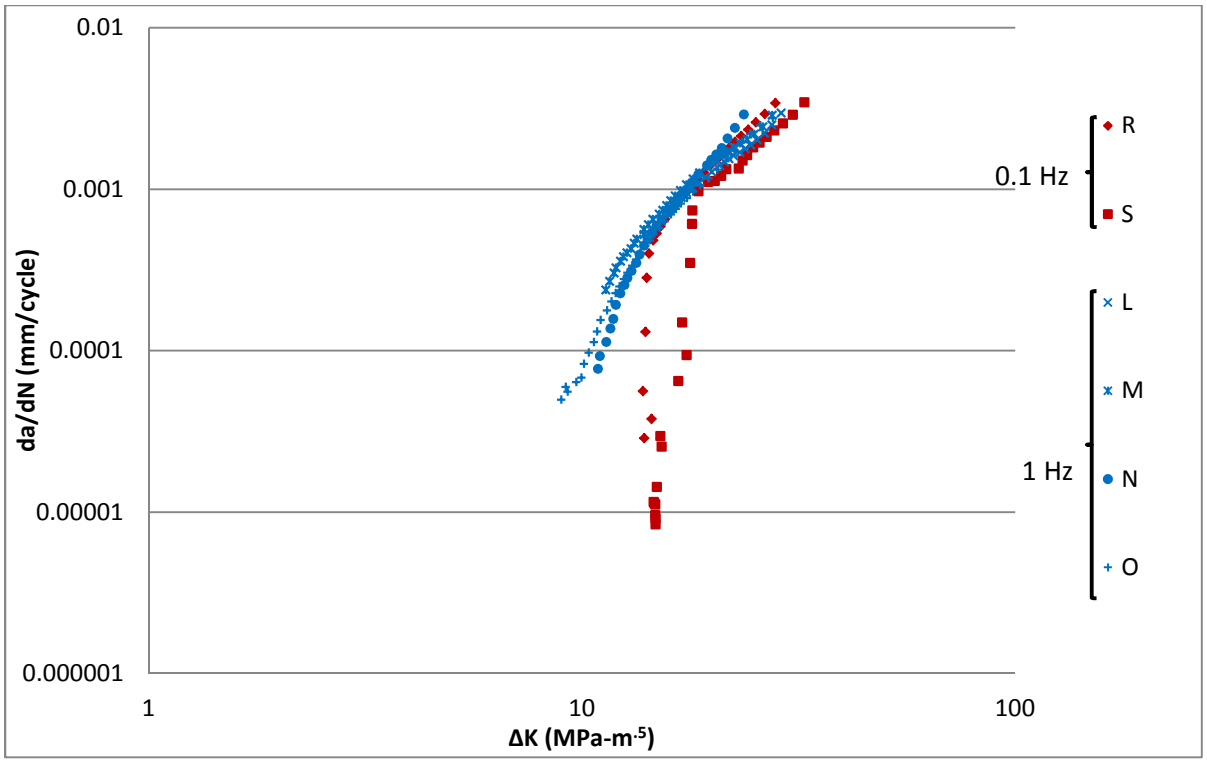

Figure 6 Specimens from Supplier A that were fatigued in 5000 psi H2 at two different frequencies and a stress ratio of 0.5. Specimens were arbitrarily labeled L-T.

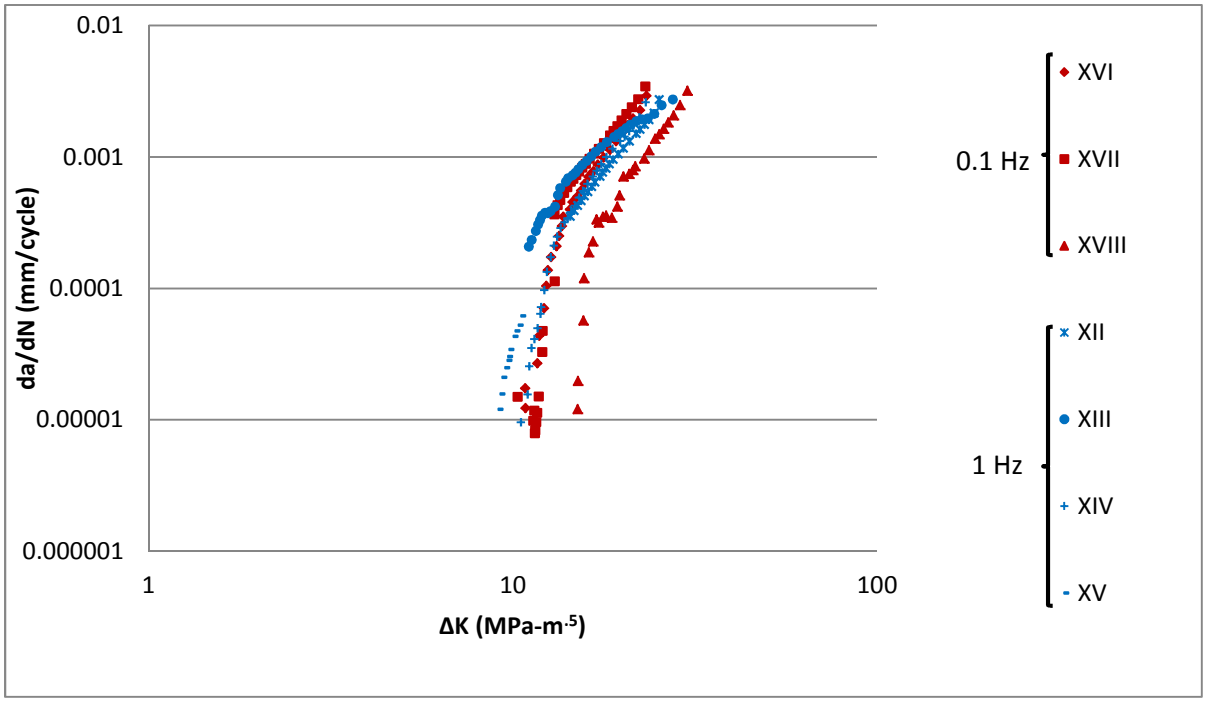

Figure 7 Specimens from Supplier B that were fatigued in 5000 psi H2 at two different frequencies and a stress ratio of 0.5. Specimens were arbitrarily labeled XII-XVII.

3.3 Impact of Microstructure

The steel provided by Supplier A had an acicular ferrite microstructure, while that provided by Supplier B had a ferrite pearlite microstructure. Pearlite blocks in ferrite pearlite impede hydrogen diffusion (36) (37), such that diffusion may occur primarily through the ferrite pearlite interfaces or through the ferrite grains (36) (38). The rate of hydrogen diffusion through ferrite pearlite steel can therefore be expected to be lower than it is in pure ferrite. The amount of hydrogen that reached crack tips and caused accelerated crack growth in the current research was therefore expected to be greater in steels provided by Supplier A than it was in those provided by Supplier B.

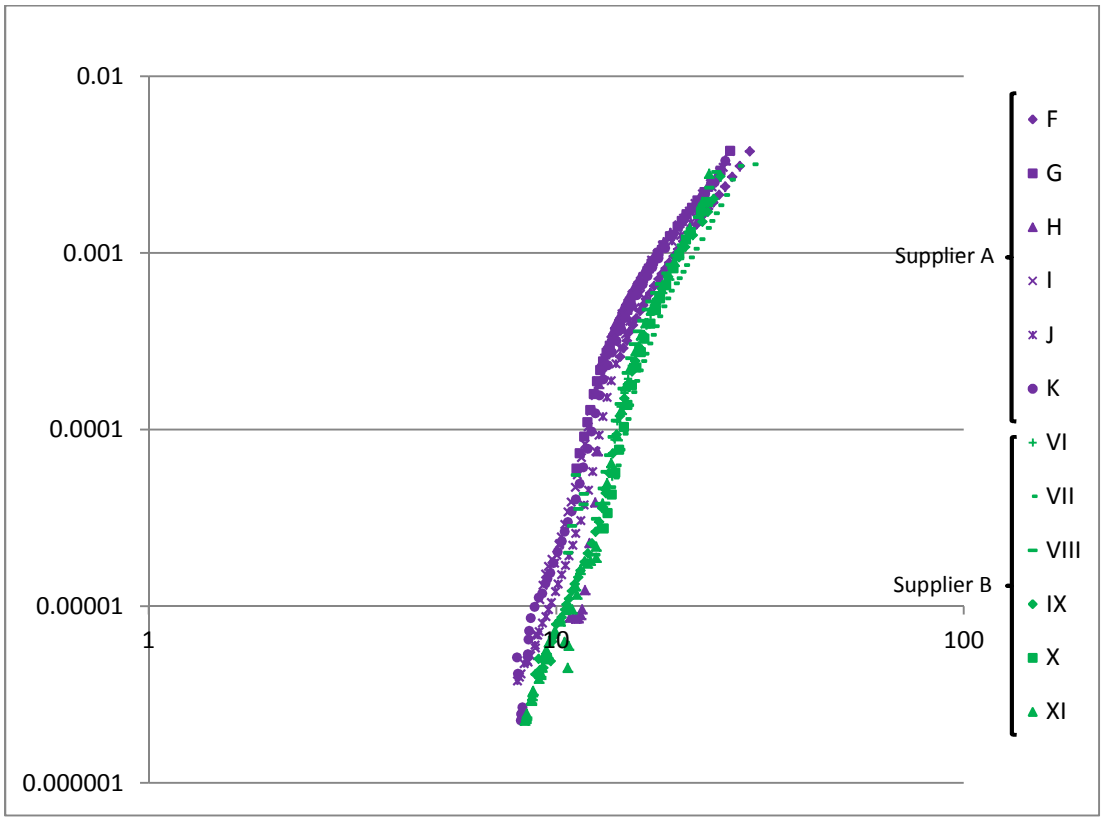

Figure 8 Specimens from Suppliers A and B that were fatigued in 800 psi H2 at 1 Hz and a stress ratio of 0.5. Specimens from Supplier A were arbitrarily labeled F-K, and those from Supplier B were arbitrarily labeled VI-XI.

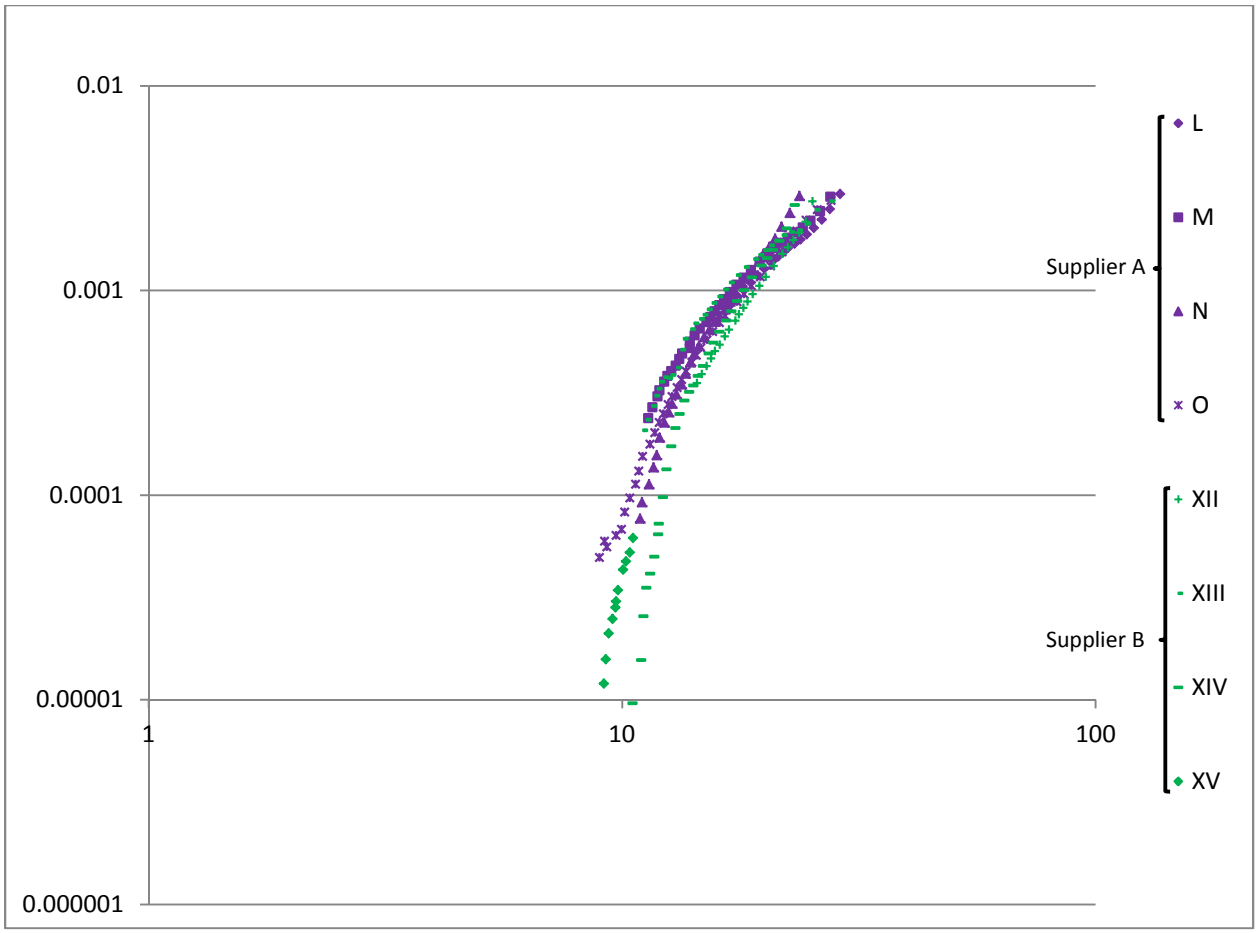

Figure 9 Specimens from Suppliers A and B that were fatigued in 5000 psi H2 at 1 Hz and a stress ratio of 0.5. Specimens from Supplier A were arbitrarily labeled L-O, and those from Supplier B were arbitrarily labeled XII-XV.

At 800 psi, crack growth rates in the acicular ferrite specimens were clearly faster than they were in the ferrite pearlite specimens. The microstructure did not have a significant effect on crack growth rates at 5000 psi, however.

3.4 Discussion

While a hydrogen pressure of 800 psi markedly enhanced crack growth rates above their values in air, increasing the hydrogen pressure above 800 psi only influenced crack growth rates in the beginning of the Paris regime of crack growth; toward the end of the Paris regime, the 800 psi and 5000 psi crack growth rate curves of specimens from both suppliers coalesced. The reason that the effect of hydrogen pressure diminished toward the end of the Paris regime may be that, at higher stress intensity

ranges, less hydrogen was able to diffuse through the specimens fast enough to reach crack tips and accelerate crack growth; the conclusion that hydrogen can not diffuse fast enough to reach crack tips during rapid crack growth was also made in (33).

Lowering the frequency of loading from 1 Hz to 0.1 Hz in 5000 psi of hydrogen appeared to have a minimal effect, if any at all, on crack growth rates in specimens from both suppliers. The reason for the absence of an effect may have been that, at 5000 psi and 1 Hz, the supply of hydrogen to the specimens was so high that the limiting steps in hydrogen assistance of crack growth were the hydrogen transport to the crack tip and the subsequent hydrogen induced damage to the crack domain. Since lowering the loading frequency merely enhances the supply of hydrogen to the crack surfaces, a reduced frequency of 0.1 Hz may not have made a difference if the supply had already plateaued at 5000 psi and 1 Hz. Modeling of environmental effects on fatigue in (35) was based on a similar premise that environmental effects on crack growth diminish in conditions wherein a combination of low cycling frequencies and high environing pressures saturate the cracked specimens.

Moreover, it is possible that, in the 5000 psi specimens, fatigue effects that cause crack growth rates to *increase* with frequency dominated the reduction in environmental effects caused by increasing the frequency. Fatigue crack growth rates in stainless steel increased with frequency at certain ΔK values in (39), and this increase was hypothesized to have been due to lower values of stiffness at crack tips being cycled at higher frequencies, enhanced crack closure at lower frequencies (due to enhanced plasticity, oxides, and roughness at the crack tip), and enhanced formation of “secondary cracks and microcavities” (39) at lower frequencies due to greater environmental effects; these “secondary cracks and microcavities” (39) may dissipate plastic energy and thereby have a net effect of impeding crack growth rather than accelerating it. Reduction in crack tip stiffness, or “crack tip softening”, is commonly observed in polymers due to an increase in crack tip temperatures during cycling (40). In order to assess

whether crack tip softening occurred in the present research, the temperatures of crack tips and surrounding plastic regions would have to be measured during fatigue. Assessment of the extent to which crack closure, microcavities, and secondary cracks could have impacted fatigue of specimens in the present study would require detailed microscopy of the specimens' fracture surfaces.

Varying the microstructure from ferrite pearlite to acicular ferrite clearly accelerated crack growth rates for most of the Paris regime observed at 800 psi, but did not have a significant effect on Paris regime crack growth rates at 5000 psi. The reason for the acceleration of crack growth at 800 psi may be that hydrogen diffusion is more rapid through acicular ferrite than it is through ferrite pearlite, as discussed in Section 3.3 (37) (36). Moreover, acicular ferrite has been theorized to more efficiently reversibly trap hydrogen than degenerate pearlite. (41) More hydrogen can therefore be expected to reach crack tips and damage the surrounding steel in acicular ferrite than in ferrite pearlite steel, resulting in faster crack growth.

In ferrite pearlite steels, hydrogen assisted fracture has been thought to occur at the boundaries between pearlite and ferrite grains (42), which are thought to be the primary hydrogen trapping sites (38) (36). The propensity for fracture along ferrite pearlite interfaces is further bolstered by indications that the cleavage fracture stress of ferrite is actually about 1.6 times that of pearlite (42), and by experimentation showing that hydrogen induced stepwise cracking in ferrite pearlite steel tends to occur along ferrite pearlite bands (36). Increasing the degree of pearlite banding has moreover been shown to enhance hydrogen induced cracking in steel under given hydrogen charging conditions (43). High concentrations of trapped hydrogen moreover often cause enough stress to build up in steel that the steel blisters. Such blistering has been observed at the surfaces of ferrite pearlite steel, where large concentrations of hydrogen build up at the ferrite pearlite interfaces, presumably because hydrogen diffusion is being blocked by the pearlite bands (36). In the current research, the hypothesis that the

ferrite pearlite microstructure was responsible for slower crack growth rates in the Supplier B steel at 800 psi could be bolstered if micrographs of the Supplier B steel specimens' fracture surfaces show blistering or stepwise cracking along ferrite pearlite bands.

In the latter part of the Paris regime, varying the microstructure stopped having an effect on crack growth rates at 800 psi. The reason that the effect of microstructure diminished at these high stress intensity factor ranges may have been similar to the reason that varying pressure did not affect crack growth rates in this part of the Paris regime. In this part of the Paris regime, hydrogen likely could not diffuse fast enough to reach the rapidly advancing crack tip, and the amount of hydrogen at the crack tip was thus determined more so by the rate at which the crack was growing per cycle than the rate of hydrogen diffusion or the environing hydrogen supply; increasing the rate of diffusion from its value in acicular ferrite to its value in ferrite pearlite may have therefore been unable to have much effect on hydrogen induced damage at the crack tips. The reason that varying microstructure did not appear to significantly impact any part of the Paris regime at 5000 psi may be that, at 5000 psi, the supply of hydrogen was so high that the lattices in both sets of steels filled rapidly enough that differences in the rates of diffusion had an insignificant impact on the acceleration of crack growth. In these experiments, the limiting step in crack growth acceleration may have been damage of the lattice by accumulated hydrogen, rather than the actual accumulation of hydrogen. The diminishing effect of diffusion rate as the supply of hydrogen is increased was similarly seen in (36), wherein ferrite pearlite steel was electrochemically charged with hydrogen and diffusion rates were measured in different directions. While hydrogen transport was faster in certain directions, after specimens were charged for 8 hours, they had similar hydrogen contents in all directions, indicating that the rate of diffusion ceased to matter after a given threshold concentration was reached in the lattices.

In conclusion, the extent to which hydrogen accelerates fatigue crack growth in a given specimen of steel is based on an interplay between the magnitude of hydrogen supply, as is determined by loading frequency and environing hydrogen pressure, and the abilities of hydrogen to reach and cause damage at crack tips in the steel, as is determined by the rate of hydrogen diffusion and the rate of crack growth. The effects of the variables studied in the current research are summarized in Table 3 below.

Table 3 Summary of Effects Analyzed in Fatigue Crack Growth Experimentation

Variable	**Effect on Fatigue Crack Growth Rate**
Increase in Pressure	↑
Increase in Frequency	↓
Increase in % Acicular Ferrite Microstructure	↑
Increase in % Ferrite Pearlite Microstructure	↓

4 Finite Element Analysis

Numerical methods are of great value in the study of hydrogen induced damage because of the complex, heterogeneous manner in which hydrogen impacts materials. Any predictive model of hydrogen induced damage must account for the influence of material properties, such as yield strength and microstructure, as well as for the variable effects of elastic and plastic deformation of the material. Elastic deformation generates hydrostatic stresses, which drive diffusion toward lattice sites by locally lowering the hydrogen's chemical potential. Plastic deformation alternatively generates trapping sites where hydrogen from surrounding lattice sites accumulates and becomes irreversibly trapped. The strain rate of a material can significantly impact the relative concentrations of hydrogen in each of these sites (44), and the manner in which the material is being loaded determines the extent of elastic and plastic deformation it incurs. Several finite element analyses have been conducted to date modeling the distribution of hydrogen in elastic-plastic materials being mechanically strained (44) (45), and the nucleation of voids and growth of cracks due to hydrogen's effect on plasticity and cohesion in a lattice (10) (22); simulations of void nucleation and crack growth have involved the development and implementation of traction separation laws that define the stress that must be applied to a lattice in hydrogen for decohesion to occur (10) (22). Such models can shed light on the mechanism of hydrogen induced damage, and can additionally be used in predictions of the likelihood of hydrogen induced damage in materials with known properties under specified operating conditions. Such models can also alternatively also be used to ascertain the operating conditions and material properties that are most likely to prevent hydrogen from damaging a material.

ABAQUS is an extremely powerful multiphysics finite element software with the ability to model mass diffusion and fatigue loading. The goal of the current research is to integrate a mechanical fatigue model with a hydrogen diffusion model to generate a simulation of fatigue crack growth and pressure-

driven hydrogen diffusion; the model is to serve as a proof of concept. As is detailed below, the model first determines the extent of crack growth and the hydrostatic stress distribution that would develop in a cracked material at the end of a series of fatigue loading cycles. Second, the model determines the distribution of hydrogen that develops in the material if it is placed in a hydrogen environment during this final state of hydrostatic stress. This model can be expanded in the future to account for the formation of hydrogen trapping sites in regions with plastic deformation. Accurate modeling of hydrogen distribution requires accounting of these trapping sites, as they may have a much greater impact on hydrogen distribution than does hydrostatic stress (45). The model should additionally be further developed such that it couples fatigue loading with hydrogen diffusion, rather than simulating these two phenomena in succession. Once these simulations are coupled, the model should be further modified such that it continuously modifies material properties, such as yield strength and lattice cohesion, as a function of internal hydrogen concentration, as was done in (10). Once the model has been expanded with all of these features- hydrogen trapping, hydrogen diffusion during fatigue, and hydrogen induced damage- hydrogen assisted fatigue crack growth could be accurately modeled in ABAQUS. Such modeling of large numbers of cycles at various frequencies would be much simpler in ABAQUS than it is in other finite element packages because of the unique cyclic modeling and multiphysics capabilities that ABAQUS has built in.

4.1 Structure of an ABAQUS Model

The two primary means of using ABAQUS to generate analyses are through input files and through the graphic user interface, known as the Complete ABAQUS Environment (CAE). Input files contain the code that ABAQUS uses to build and run a model. The input files can be generated in a text editor, or can alternatively be generated through the CAE. The majority of the current work was done via the CAE. Modification of the CAE-generated input files using text editors was performed when

features that were not supported by the CAE were being modeled, such as the criteria for crack propagation in low cycle fatigue.

An ABAQUS model has several different components. The model geometry is defined by entities known as parts, which are discretized into units known as elements. The elements are comprised of nodes, and "are connected to one another by shared nodes" (46). The elements collectively form the part's 'mesh'. Each element available in ABAQUS has a unique combination of the following properties: geometry, degrees of freedom, number of nodes, formulation, and method of integration. Elements are categorized into families, where the family defines the element's geometry and degrees of freedom. The 'formulation' of the element refers to whether the element has nodes only at its corners or additionally has nodes in between corners, and, consequently, whether the element uses linear or quadratic integration, respectively. In stress analyses, the type of integration can further be specified as full or reduced. Reduced integration uses one less node than full integration, and is sometimes appropriate in the modeling of flexibility in certain mechanical analyses.

Once a model part is generated, loads and boundary conditions can be applied to the part. Boundary conditions specify the values of degrees of freedom at given nodes (where those values are known). Convergence of a model's analysis often requires that it have boundary conditions. Additionally, before an analysis is run, the model part is associated with a user-specified material, which defines the properties of the part that are relevant to the analysis being run.

4.2 Stress-assisted Hydrogen Diffusion in ABAQUS

This work modeled stress-assisted hydrogen diffusion by generating two separate simulations (a mechanical simulation and a diffusion simulation) in ABAQUS. Integration of the two analyses was performed by passing the hydrostatic stress values determined by the mechanical simulation into the diffusion simulation. While the model would have been far more accurate if both analyses were

conducted in a single simulation, they could not be integrated because the elements that allow the simulation of mass diffusion using the diffusion analysis feature built in to the ABAQUS CAE do not additionally allow simulation of mechanical loading. Fatigue and mass diffusion have been integrated in past studies, such as (22), but doing so requires the manipulation of subroutines in ABAQUS; this was outside of the scope of the current research. Specimen geometries and mesh sizes in both simulations were identical, except that the specimen used in the diffusion analysis did not have a crack. Cracks cannot be modeled with the elements that can model mass diffusion in the ABAQUS CAE. However, as is discussed in Section 4.3.3.3, the absence of the crack did not influence the locations or identification numbers of the nodes in the diffusion specimen. The specimens in the diffusion analysis and fatigue analysis had identical node identifiers and locations. The geometry of the specimen and its mesh are shown in Figure 10 below.

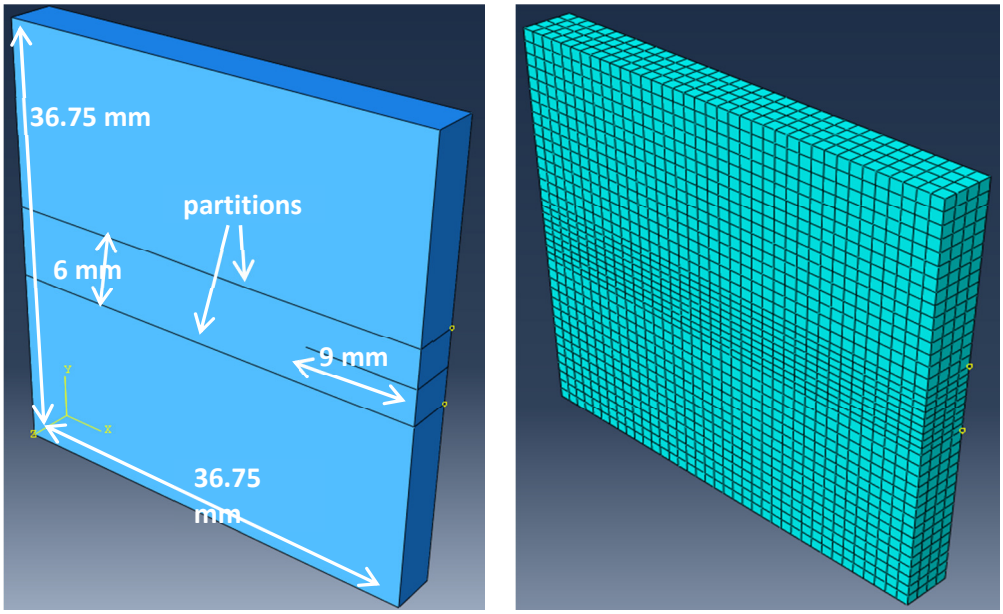

Figure 10 Part geometry (left) and mesh (right) for mechanical and diffusion analyses

The specimen geometry was intentionally chosen to be free of discontinuities, with the exception of the crack, and to have a small volume. Generating solutions for an analysis with more discontinuities or a

greater volume would have required a substantially finer mesh, and the ABAQUS teaching license that was used to conduct modeling limits models to 20,000 nodes. The "partition" feature in ABAQUS was used to refine the region of the mesh within a region 3 mm above and below the crack. All of the meshed elements used in simulations were shaped as bricks. The elements in the unrefined region had lengths of 0.001 m on all sides, and the elements in the refined region had lengths of 0.0007 m on all sides.

Fatigue loading was applied to the first simulation, and the final hydrostatic stress values at each of the nodes in the mesh were output by ABAQUS into a results file. These stress states were then input to the second model, and a hydrogen concentration was applied to the specimen surface in the second model. Hydrogen diffusion through the specimen was then simulated in the second model, and, as would be expected, the hydrogen diffused toward the location of the stressed crack tip, as determined by the hydrostatic stress gradients supplied by the first model. The input files necessary to run the fatigue and diffusion analyses are provided in Appendices A and B, respectively.

4.3 Stress Analysis

4.3.1 Element Type

The C3D8 element was used for the stress analysis. This element is a fully integrated, linear, three-dimensional, 8-node brick of the continuum family. Continuum elements were used because they can model a variety of different geometries and mechanical loads, as they "have translational degrees of freedom at each node" (46). Other element families such as beams and trusses, can also model stress, but are only appropriate under very specific geometries or loading conditions that either require their use or would be more economically simulated by elements from those families. Continuum elements are widely used in stress analyses, and are appropriate when a model does not have unique properties (such as negligible thickness or resistance to bending). Brick shaped elements were chosen because,

with the same number of nodes, they yield more accurate results than their alternatives (wedge and tetrahedral shapes). Wedge and tetrahedral shapes require fine meshing to attain accurate results, and are most commonly used when they are necessary due to complex geometries. Fully integrated linear elements were chosen because "only first order solid continuum…elements and second order stress/displacement tetrahedron elements" (46) can be used to model a crack domain in the extended finite element method, which will be discussed in Section 4.3.3.3. The main advantage of second order elements over first order elements is that they are likely to be more accurate under bending loads; since the current model involves minimal bending, linear elements are likely to be sufficiently accurate. Full integration over linear integration was utilized because reduced integration schemes often cause linear elements to behave too flexibly, yielding inaccurate results. (46)

4.3.2 Material Properties

Several models that define the elastic-plastic behavior of a material are built in to ABAQUS. The current analysis uses the Ramberg-Osgood model, as it is commonly used to define the full mechanical behavior of ductile metals, such as steel. The one-dimensional Ramberg-Osgood model is:

$$E\varepsilon = \sigma + \propto \left(\frac{|\sigma|}{\sigma_0}\right)^{n-1} \sigma, \quad \textbf{9}$$

Where σ is the stress tensor, ε is the mechanical strain tensor, E is Young's modulus, α is a material specific constant, σ_0 is the yield stress, and n is a hardening exponent. (46)

ABAQUS then generalizes this one-dimensional model into multiple axes using Poisson's ratio and the Mises stress potential (46), as is shown in Equation 10 below:

10 $E\varepsilon = (1+v)[S] - (1-2v)p[I] + \frac{3}{2}\left(\propto \frac{q}{\sigma_0}\right)^{n-1}[S]$,

Where E is Young's Modulus of Elasticity, ε is the strain tensor, v is Poisson's ratio, [S] is the stress deviator, p is hydrostatic stress, α is a material specific constant, q is the Von Mises equivalent stress, σ_0 is the yield stress, and n is a hardening exponent. (47)

In Equation 10, the hydrostatic stress is determined by:

11 $p = -\frac{1}{3}[\sigma]:[\sigma]$,

Where σ is the stress tensor (47),

the Von Mises Equivalent stress is determined by:

12 $q = \sqrt{\frac{3}{2}[S]:[S]}$,

Where S is the stress deviator (47),

and the stress deviator is determined by:

13 $[S] = [\sigma] + p[I]$

Where σ is the stress tensor and p is the hydrostatic stress. (47)

Additionally, because the specimen in this model has a crack with the potential to grow, it was required by ABAQUS that criteria be specified for damage initiation and evolution upon the application of stress. When the damage initiation criterion is satisfied anywhere in the crack domain, either the existing crack will grow or a new crack will nucleate (depending on where in the domain the criterion is satisfied- at the crack tip or elsewhere). ABAQUS has several different options for damage criteria. This analysis defined damage initiation by the "maximum principal stress criterion" (46), according to which a

crack will nucleate when the principal stress experienced at a given node reaches the user-specified maximum principal stress. While this criterion is not necessarily the most accurate, it was used in this analysis because criteria were subsequently specified for damage in low cycle fatigue (as will be discussed later), and fatigue is expected to be the primary damage mechanism in the current simulation. Consequently, any criterion for damage through an alternative stress state (tension, compression, etc.) is not expected to ever be met.

The damage evolution criterion describes the stress strain behavior of the material after yielding. The stress strain behavior after yielding can be defined as linear or exponential, and can be calculated based on energies or displacements. Since the Benzeggagh-Kenane (BK) Law was used in this model to define the conditions of fatigue crack growth (as will be discussed later), and the BK Law is based on energies, damage evolution was also defined based on energies for consistency. For sake of simplicity, the damage evolution was defined as linear. This simulation should be modified in the future based on experimental data on the stress strain behavior of steel. Such experimental data could be used to determine whether damage evolution simulation is more accurate when based on energies or on tractions, and also to determine the value of the exponent in the exponential damage evolution criterion. (46)

In order to model crack growth in fatigue, ABAQUS additionally required that the Mode I, II, and III critical energy release rates, the ratios $\frac{G_{threshold}}{G_C}$ and $\frac{G_{pl}}{G_C}$, the BK Law constant (for mixed mode loading), the constants c_1 and c_2 in a fatigue initiation criterion, and the constants c_3 and c_4 in a modified version of the Paris Law be specified. Definitions of these terms and the manner in which they are used as crack growth criteria are discussed in Section 4.3.3.2.

Since the model was intended solely to serve as an initial proof of concept, values for the aforementioned material properties were taken from published literature. If this model were to be used

for predictions of actual behavior, however, all of the above properties would have to be determined through experimentation on the material being studied. Some properties, such as the critical energy release rates, would have to be determined directly, and others, such as the BK Law constant, could then be derived given their known relationships with the properties that were determined experimentally.

The material properties used in the model are provided in Table 1.

Table 4 Material Properties

σ_{YS}[1] (yield stress) (MPa)	350.9
α[1]	3.143
n[1]	8.072
Young's Modulus[1] (GPa)	207
Poisson's Ratio[2]	.3
Maximum principal stress (MPa)[1]	350.9
G_{Ic} (Mode I Critical Energy Release Rate)[3] (MPa-m)	.011271
G_{IIc} (Mode II Critical Energy Release Rate)[4] (MPa-m)	.04438
G_{IIIc} (Mode III Critical Energy Release Rate)[5] (MPa-m)	.106348
BK Law constant η[6]	1.8
$\frac{G_{threshold}}{G_c}$ ratio[7]	.01
$\frac{G_{pl}}{G_c}$ ratio[7]	.85
c_1 constant[8]	.5
c_2 constant[8]	-1.44
c_3 constant[9]	7.74412E-5
c_4 constant[9]	2

Notes:

1 Source: (48)

2 Source: (49)
3 Source: (50)
4 Source: (51)
5 Source: (52)
6 Could not be found for steel. This is the exponent for AS4/3501-6 carbon epoxy. Source: (53)
7 ABAQUS default values
8 Could not be found for steel. This is the exponent for a double cantilever beam described in ABAQUS example files. Source: (46)
9 Source: (49)

4.3.3 Fatigue Analysis

In order to simulate fatigue loading of this specimen, the fatigue and extended finite element method (XFEM) analysis features that are built in to ABAQUS were used. The model simulates fatigue crack growth through a combination of three processes: analysis of a material's stabilized responses to cyclic loading, analysis of the damage a material incurs during a series of cyclic loadings, and XFEM-based crack growth. Each of these processes and the manner in which they collectively simulate fatigue crack growth are described below.

4.3.3.1 Direct Cyclic Analysis Algorithm

In the simulation of fatigue, ABAQUS discretizes the total number of loading cycles being applied into sets of cycles, and the material's stress-strain behavior during each set of cycles is assumed to stabilize to a constant response. The manner in which the loading cycles are divided is discussed in Section 4.3.3.2.

One way to determine the stable stress-strain response of a material to cyclic load is to calculate the material's response to each loading cycle that is applied. This method is extremely computationally intensive, however, and ABAQUS thus instead uses Newton iteration to solve for the unknown displacement coefficients in the following truncated Fourier Series representing the material's displacement:

$$\textbf{10}\quad u(u_0, u_k^s, u_k^c, t) = u_0 + \sum_{k=1}^{n}[u_k^s \sin k\omega t + u_k^c \cos k\omega t],$$

Where t is time, n is the number of terms in the Fourier Series, ω is the angular frequency, and u_0, u_k^s, and u_k^c are unknown displacement coefficients. u_0, u_k^s, and u_k^c are constants, but have been written as variables in Equation 10 because they will be solved for using Newton Iteration, wherein they will be treated as variables. (46)

The angular frequency, ω, is defined by:

$$\textbf{11}\quad \omega = \frac{2\pi}{T},$$

Where t is time and T is the period of u(t), such that u(t+T) = u(t). (46)

This process of Newton Iteration entails representing the system of equations being solved for, $u(u_0, u_k^s, u_k^c, t)$, as a vector of equations:

$$\textbf{12}\quad u(u_0, u_k^s, u_k^c, t) = \left(\begin{bmatrix} u(u_0 \ldots) \\ u(u_k^s, \ldots) \\ u(u_k^c, \ldots) \\ \vdots \end{bmatrix}\right)$$

$u(u_0, u_k^s, u_k^c, t)$ has a value of 0 during every cycle (when unloading of the specimen is complete). When $u(u_0, u_k^s, u_k^c, t)$=0, the equilibrium condition sought by the algorithm is met when the following equation is minimized within a specified tolerance:

$$\mathbf{13}\quad R(u_0, u_k^s, u_k^c, t) = J \times d(u_0, u_k^s, u_k^c, t)$$

Where $R(u_0, u_k^s, u_k^c, t)$ is the vector of residual errors, J is the Jacobian matrix, and $d(u_0, u_k^s, u_k^c, t)$ is a vector containing the increments by which each of the input variables being solved for was modified in the given iteration. The Jacobian matrix in Newton iteration of the $u(u_0, u_k^s, u_k^c, t)$ system of equations is the elastic stiffness matrix.

The equilibrium condition is then iteratively solved for until the residuals are minimized within a prescribed tolerance. This iteration method is particularly efficient because the Jacobian matrix remains constant throughout all of the cycles, and thus does not need to be repeatedly recalculated. The current analysis allowed ABAQUS to automatically select the number of iterations that it conducted as well as the number of Fourier coefficients it used. (46) (54) (55)

In the current analysis, ABAQUS was allowed to determine the number of terms to include in its Fourier Series representation of the displacement function. Including more terms within the series makes the solution more accurate, but also makes it more computationally intensive, thereby increasing the amount of time required for convergence. The ABAQUS default setting was used, which starts with 11 terms and then adds 5 terms at a time when necessary. Terms are added only if the solution for the displacement function over a given period of time has converged, but had previous time points at which convergence was not attained. The maximum number of terms ABAQUS will include in the default setting is 25.

4.3.3.2 Fatigue Damage

ABAQUS models fatigue crack growth by dividing the entire set of loading cycles into sets of cycles, and then assuming that the response of the material during each set will stabilize, such that it can be predicted by the direct cyclic analysis approach detailed in Section 4.3.3.1. At the end of a cycle

set, the damage the material has incurred during that cycle set is calculated, and the material properties are updated. These new properties are then used during the next cycle set, and the stabilized cyclic response during that set is calculated just as it was for the first set. In this way, the response of the material at any point in the fatigue loading is approximated. (46)

ABAQUS determines the number of loading cycles in each of these cycle sub-sets in the following manner. ABAQUS first checks to see if the two criteria for crack initiation are met in the specimen:

$$\mathbf{14} \quad G_{max} > G_{threshold}$$

where G_{max} is the maximum energy released during a cycle and $G_{threshold}$ is the energy release rate below which fatigue crack growth can be presumed not to occur, and

$$\mathbf{15} \quad \frac{N}{c_1 \Delta G^{c_2}} \geq 1$$

where N is the cycle number, ΔG is the energy release rate during a cycle of fatigue and c_1 and c_2 are material-specific constants.

If both of these criteria are met, ABAQUS will either nucleate a crack or grow an existing crack. If the criteria are met, ABAQUS first determines the direction in which the crack is most likely to grow, and then calculates the number of cycles that each of the elements ahead of the crack would need to have transpired before the respective element fractures into two pieces, using Equation 16 below. The element that requires the smallest number of cycles to fracture completely, N, is then chose to be the next element the crack will traverse, and the size of the next set of loading cycles is now established as N. The direct cyclic analysis approach (detailed in Section 4.3.3.1) is then used to determine the stabilized cyclic response of the material during this set. The user can specify the maximum value for N.

This default maximum value of 501 cycles was used in this analysis. The value of N is determined using a modified version of the Paris Law:

$$\textbf{16}\quad \frac{da}{dN} = c_3 \Delta G^{c_4}$$

Where da/dN is the crack growth rate per cycle, c_3 and c_4 are material-specific constants, and ΔG is the energy release rate during a cycle of fatigue. (46)

At the end of the last stabilized loading cycle in the set of N cycles, ABAQUS repeats the above process, again determining the direction of likely crack growth and then calculating a new value for N.

In order for ABAQUS to simulate fatigue, the user must specify several material-specific constants that are usually determined experimentally. These constants are:

- Critical energy release rates in each mode of loading, G_{IC}, G_{IIC}, and G_{IIIC}

  The critical energy release rate is the energy release rate at which a material will fracture
- Material-specific constants for one of the three mixed mode fracture laws ABAQUS offers to determine the critical fracture energy release rate, G_c, of a material in mixed mode loading. The laws built in to ABAQUS are: the BK Law, the Power Law, and the Reeder Law. The BK Law was chosen for this analysis and is defined as:

$$\textbf{17}\quad G_c = G_{IC} + (G_{IIC} - G_{IC}) \left(\frac{G_{II}+G_{III}}{G_I+G_{II}+G_{III}}\right)^{\eta}$$

  where G_{IC}, G_{IIC}, and G_{IIIC} are the user-defined critical energy release rates in Modes I, II, and III loading, respectively; G_I, G_{II}, and G_{III} are the ABAQUS-determined energy release rates in Modes I, II, and III loading, respectively; η is a material-specific constant.
- The ratio $\frac{G_{threshold}}{G_c}$, where $G_{threshold}$ is the energy release rate below which fatigue crack initiation or growth can be presumed not to occur.

- The ratio $\frac{G_{pl}}{G_c}$, where G_{pl} is the energy release rate above which a crack will grow in fatigue at an accelerated rate. (46)
- The constants c_1 and c_2 in Equation 15.
- The constants c_3 and c_4 in Equation 16.

4.3.3.3 Extended Finite Element Method (XFEM)

Modeling crack growth in a finite element analysis using traditional methods is difficult and cumbersome because the crack tip creates a tremendous discontinuity in the finite element mesh. Convergence of the analysis thus requires the mesh around the tip to be made extremely fine, and, as the crack grows, for the mesh to be repeatedly refined in the region of the crack tip. ABAQUS offers two means to circumvent these challenges- the extended finite element method (XFEM) and modeling with cohesive elements. XFEM is advantageous over the use of cohesive elements because it does not require the crack path to be predefined; XFEM instead allows for the simulation of "crack initiation and propagation along an arbitrary, solution-dependent path in the bulk materials" (46). This analysis therefore used XFEM to propagate a pre-existing (starter) crack in the model.

XFEM is conducted by enriching the nodes surrounding a discontinuity with additional degrees of freedom, such that their behavior is now determined by additional functions. The displacement of nodes in the enriched region is then defined as the sum of the standard finite element approximation and the 'enriched' approximation. The 'enriched' approximation is that which is made by the functions defining the additional degrees of freedom. (56) (57) (46) In ABAQUS, the displacement vector in enriched regions is thus defined as:

18 $u = \sum_{I=1}^{N} N_1(x)[U_I + H(x)a_I + \sum_{\alpha=1}^{4} F_{\propto}(x)b_I^{\alpha}]$

Source: (46)

The first term in the above summation represents the standard finite element approximation. The second term represents displacement of the crack line, where a_I is "an enriched degree of freedom vector" (46) and *H(x)* is a Heaviside function defining the crack line. The third term represents displacement of the crack tip, where b_I^{α} is an "enriched degree of freedom vector" (46) and $F_{\propto}(x)$ represents "the asymptotic functions associated with the crack tip" (57).

Accurately modeling crack growth requires constantly recalculating the third term in the above equation at the crack's current location. To avoid this cumbersome task, ABAQUS models crack growth using only the displacement across a cracked surface (the second term in the above equation). Ignoring the third term and using only the crack line requires that the crack "propagate across an entire element at a time" (46), such that the crack tip singularity never has to be modeled. When a user specified fracture criterion (ex. maximum principal stress, fatigue initiation, etc.) is satisfied within the enriched region, the nodes where the criterion is satisfied separate, creating two crack flanks. In addition to its standard nodes, each of these flanks has 'phantom nodes' that represent the nodes that previously bordered the crack but now belong to the other flank. These phantom nodes provide the degrees of freedom necessary to use a traction separation law to calculate the displacement of each of these flanks as a function of the fracture criterion. The phantom nodes have only those degrees of freedom that are necessary for this calculation, and thus become meaningless when a crack growth increment is complete and the flanks are separate. (57) (46) (58) Figure 11 below shows that a crack domain is composed of real nodes and their corresponding phantom nodes.

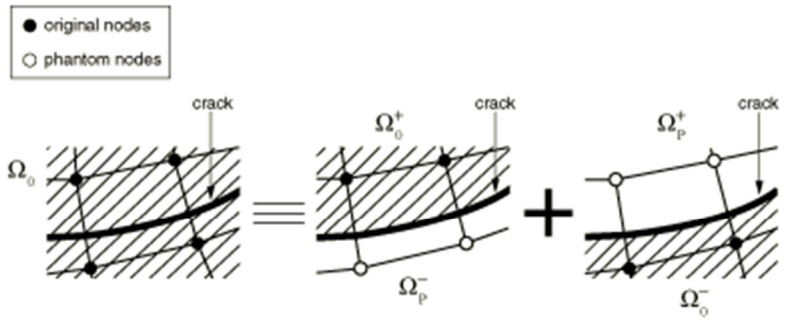

Figure 11 Phantom Nodes in ABAQUS Implementation of XFEM. Source: (46)

The phantom nodes and their corresponding real nodes separate when a crack grows, and the phantom nodes of a given crack flank are used to determine displacement of the other crack flank.

4.3.3.4 Loads and Boundary Conditions

The fatigue analysis simulated 259200 seconds, or 72 hours, of cyclic loading applied to the meshed part in the model, at a frequency of 6.28319 radians/second, or 1 Hz. The minimum load applied in any cycle was 5 kN and the maximum load was 10 kN, corresponding to a stress ratio, R, of 0.5. The loads were applied as pressures of 34 and 68 MPa, respectively, at the top and bottom surfaces of the specimen, as is shown in Figure 12 below.

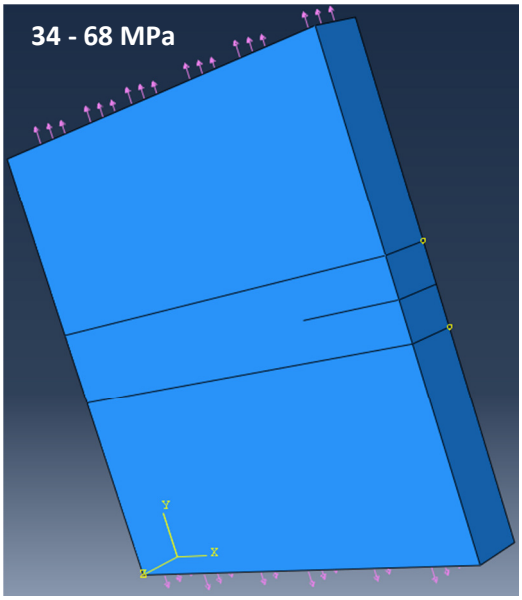

Figure 12 Cyclic Loading of Specimen

The boundary conditions applied restricted motion of the part in the z direction, and rotation of the part about the x and y axes. The specified maximum inelastic strain rate change allowable in a given increment was .001. ABAQUS automatically determined the number of increments in each set of cycles within this tolerance specification. The initial increment size was 259200 seconds, the minimum size was 0.1 second, and the maximum size was 259200 seconds.

4.3.4 Output

The stress analysis generated a results file with hydrostatic stress values at each of the nodes in the part mesh. At any given node, ABAQUS derived the value for hydrostatic stress by first categorizing all of the elements in the mesh into 'averaging regions', and then averaging all of the components of the hydrostatic stress tensor "over all of the elements" that were both connected to the node and belonged to the node's averaging region. (46) The hydrostatic stress results were subsequently input into the diffusion analysis discussed in Section 04.4 to simulate pressure-driven hydrogen diffusion.

Additionally, displacement and stress values were output to a database, such that crack growth and stress distribution could be visualized. Figure 13 below shows the hydrostatic stress distributions at

the end of the fatigue analysis detailed in Section 4.3.3.4

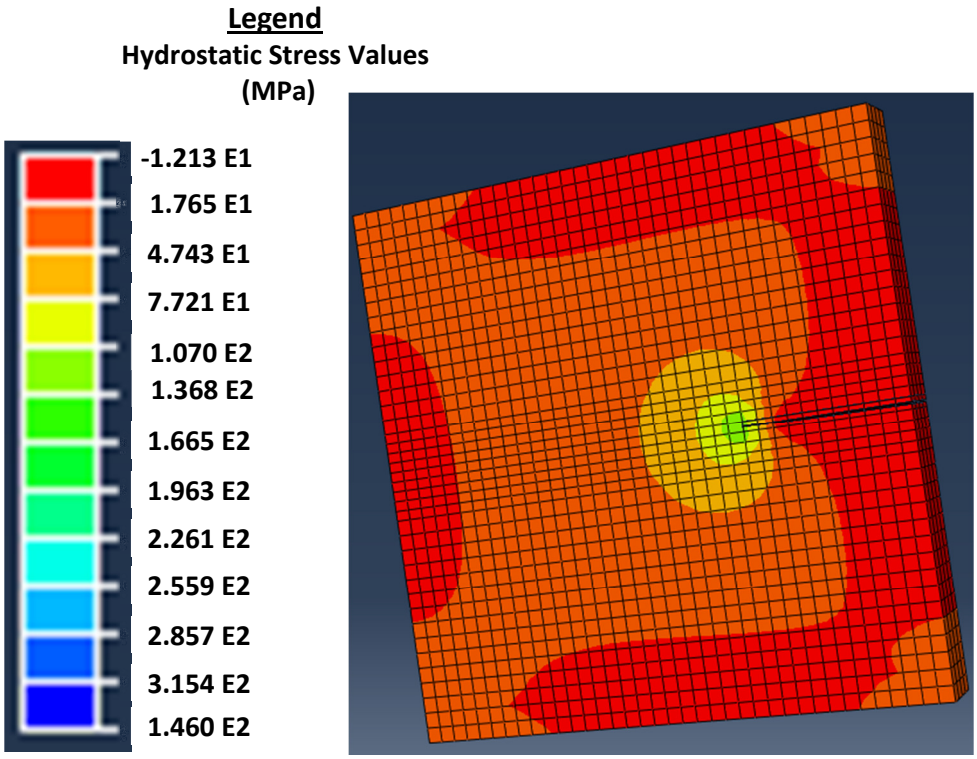

Figure 13 Hydrostatic Stress Distribution at End of 3 days of Fatigue Loading Cycles

As would be expected, circular regions of plastically deformed material developed at the crack tip, where the magnitude of hydrostatic stress was greatest. The negative hydrostatic stress values in the specimen are likely due to inaccuracies in the stress calculation that would be resolved with a finer mesh. The crack had a final length of 10.92 mm, indicating 1.92 mm of crack growth. The shape of the Von Mises stress distribution at the crack tip (Figure 14) was consistent with the distortion energy theory. (40) As would be expected, the Von Mises stress at the crack tip exceeded the material's yield stress, resulting in crack growth.

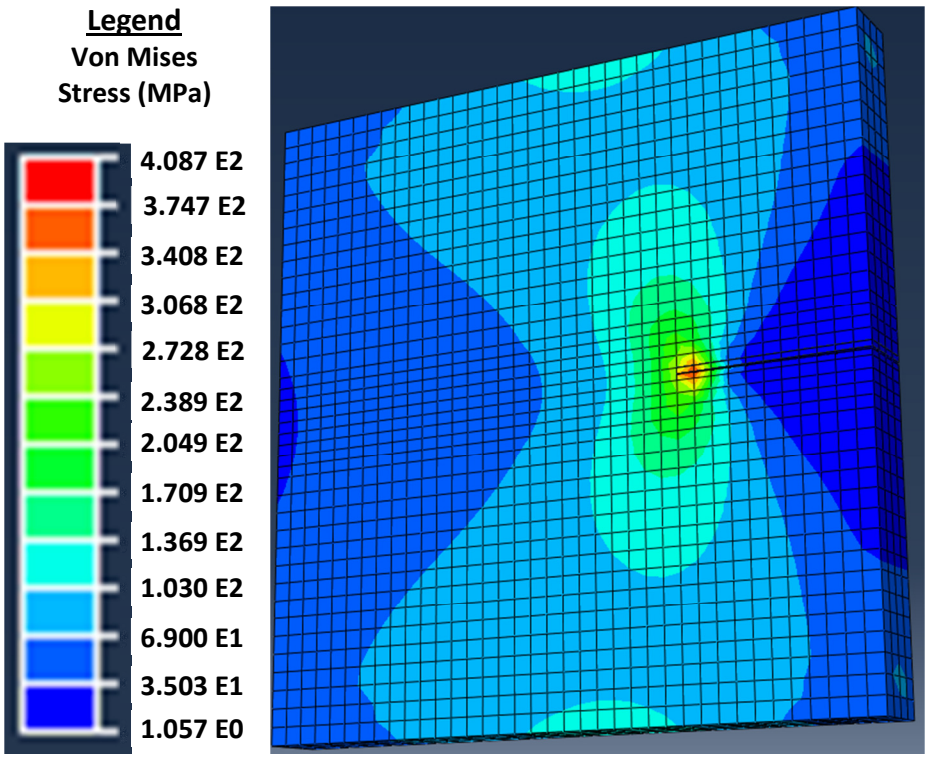

Figure 14 Von Mises Stress Distribution in Specimen after Fatigue Loading

The results of this analysis show that fatigue crack growth can be simulated in ABAQUS. It is important to note, however, that these results are not necessarily realistic, as the material properties for the analysis were drawn from numerous pieces of literature, rather than one set of experiments, and the part mesh was relatively coarse and could not be refined any further since the ABAQUS student license being used limited the user to 20,000 nodes. The hydrostatic stress values determined in the fatigue analysis were used to simulate stress-driven hydrogen diffusion, as is detailed in Section 4.4.

4.4 Diffusion Model

4.4.1 Element Type

The geometry of the specimen was identical in the diffusion and stress analyses, but the element types were different. The element used in the diffusion analysis was DCC3D8, an 8-node, linear, continuum brick. The mass diffusion law built into ABAQUS can only be used with the solid

continuum elements that have concentration degrees of freedom. The brick geometry was chosen because it was likely to be more computationally economical than wedge-shaped or tetrahedral elements, and linear integration was chosen because quadratic integration with DCC3D8 can not be conducted through the ABAQUS CAE.

4.4.2 Material Properties

The material properties that must be input to an ABAQUS model of stress-driven mass diffusion are:

- Diffusivity

  Diffusivity was assumed to be isotropic in the model, and was calculated using the following equation:

$$\textbf{19}\quad D = \frac{7.611\times10^{-8}\times e^{-1157/T}}{1+(1.05\times10^{-3}\times e^{3573/T})}\ m^2/s$$

  Where D is diffusivity and T is temperature in Kelvins (46)

- Solubility

  Solubility was calculated in the model using the following equation:

$$\textbf{20}\quad s = 4.3\times e^{-3261/T}\ ppm\ m\ N^{-1/2}$$

  Where s is solubility and T is temperature in Kelvins (46)

- Pressure stress factor

  The pressure stress factor is a constant used by ABAQUS to simulate diffusion driven by hydrostatic stress in a material. It is defined in the following equation:

$$\mathbf{21}\quad k_p = \frac{\overline{V_H} \times c}{s \times R \times T}\ m\ N^{-1/2}$$

Where k_p is the pressure stress factor, $\overline{V_H}$ is the partial molar volume of the diffusing phase in m^3/mol, c is the concentration of the diffusing phase in ppm, s is the solubility of the diffusing phase in ppm-m-$N^{-1/2}$, R is the universal gas law constant in J-mol^{-1}-K^{-1}, and T is the temperature in Kelvins

k_p must be specified in ABAQUS along with the concentration at which it was calculated.

The value of $\overline{V_H}$ in the model was 2.0 x 10^{-6} m^3-mol^{-1} (46)

- Specific Heat
- Density

The material properties input to the current model were:

Table 5 Material Properties for Diffusion Model

Temperature (K)	343.15
Universal Gas Constant (J/kg/K)	8.314
Diffusivity (m^2/s) [1]	7.272E-11
Solubility (ppm-m-$N^{-1/2}$) [1]	3.20856E-4
Pressure stress factor (m-$N^{-1/2}$)[1] and corresponding Hydrogen Concentration (ppm)	.00000164636, 0.75355 ppm
Specific Heat[2] (J-kg^{-1}-K^{-1})	490
Density[3] (kg/m^3)	7850

Notes:

1. Calculated per equations 19, 20, and 21 at a temperature of 343.15 K.
2. Source: (59)
3. Source: (60)

4.4.3 Mass Diffusion Step

"The flux of concentration of the diffusing phase" can be determined in ABAQUS using either an equation based on chemical potential or "an extended form of Fick's Law" (46). Both chemical potential and Fick's Law have been used to simulate hydrogen diffusion through steel in previous studies (22) (45). The extended form of Fick's Law was chosen for this study:

$$\mathbf{22}\quad J = -D \cdot \left(\frac{\partial c}{\partial x} + s k_p \frac{\partial p}{\partial x}\right)$$

where J is the flux concentration, D is the diffusivity of the hydrogen through steel, c is hydrogen concentration in ppm, k_p is the pressure stress factor, *s* is the solubility of the diffusing phase, and *p* is the "equivalent pressure stress"; the "equivalent pressure stress" is defined as the negative of the hydrostatic stress. (46)

The diffusion step can be either Transient or Steady State. Steady state analyses provide the steady-state solution directly, having no regard for the time length the user has specified for the mass diffusion step (46). Transient analyses instead solve for the concentration of the diffusing phase in time increments, including the rate at which concentration changes with respect to time in the governing diffusion equation (46). The degree to which inclusion of the time dependence of hydrogen concentration enhances the accuracy of a finite element model depends on the rate at which the specimen in the model is being strained. At high strain rates, hydrogen from lattice sites in a steel diffuse toward trapping sites, and environing hydrogen is thought to be unable to replenish the lattice sites as quickly as they are depleted. Consequently, hydrogen concentrations are higher at the trapping sites. At slow strain rates, the lattice sites are replenished, and the hydrogen distribution in the material has been theorized to eventually approximate steady state values. (44) Since the trapping sites were not included in the current model, the analysis was conducted for steady state conditions.

Hydrostatic stresses were read in to the diffusion model from one of the output files generated by the 3-day fatigue model. Since the mesh geometries were identical in both models (as the specimens were of identical sizes and geometries in both models, and additionally had elements with identical sizes and geometries), the node locations and numbers were also identical in both models. The nodal hydrostatic stress values at the end of the fatigue analysis were thus applied at nodes in the same relative locations in the diffusion analysis.

4.4.3.1 Load, Boundary Conditions, and Initial Conditions

Loads and boundary conditions were not necessary for the diffusion model, although hydrogen concentration can be applied as either a load or boundary condition. A hydrogen concentration of 0.75355 ppm, corresponding to an environing hydrogen pressure of 5.5 MPa or 800 psi, was applied to one surface of the specimen as an initial condition, such that the hydrogen would diffuse through the specimen during the mass diffusion step described in Section 4.4.3. The value of hydrogen concentration had to be input to ABAQUS as a 'normalized concentration', defined as:

$$\textbf{23} \quad Normalized\ concentration = \frac{concentration\ (ppm)}{solubility}$$

Source: (46)

4.5 Output

The final distribution of hydrogen in the specimen is shown in Figure 15 below. As would be expected, the hydrogen concentration is greatest where the compressive hydrostatic stresses are greatest; the crack can not be seen in this figure because crack growth can not be modeled in a diffusion analysis. These results show that a model of mechanical fatigue can successfully be integrated with a model of mass diffusion in ABAQUS. In the future, these analyses should be coupled rather than being conducted in succession, such that the dependence of diffusion on time is accounted for.

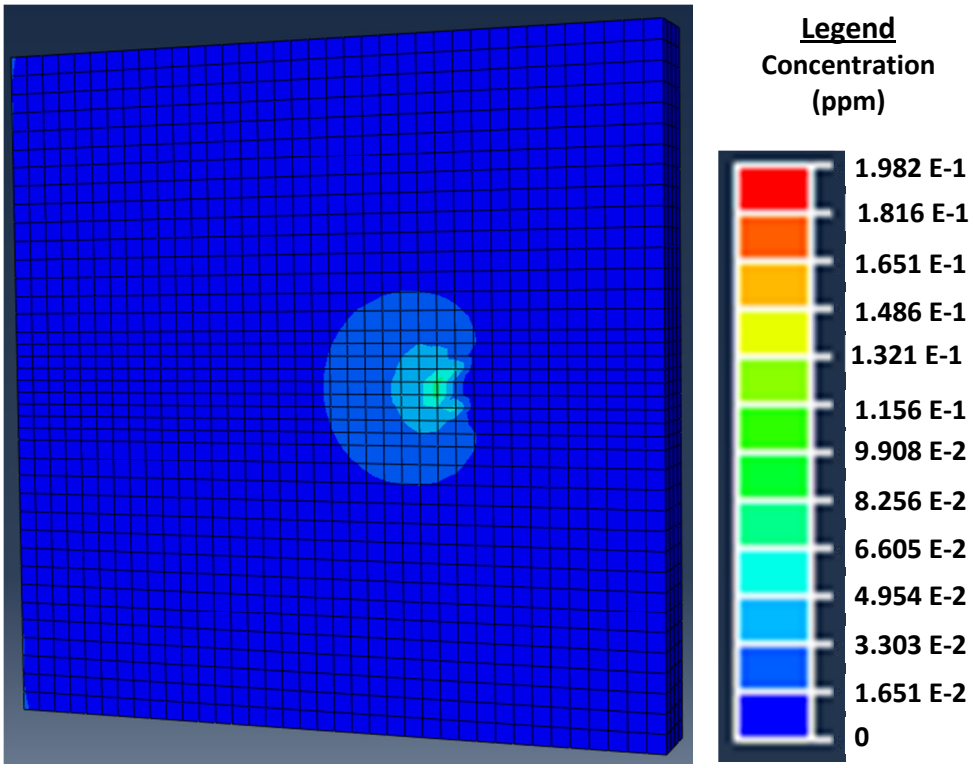

Figure 15 Hydrogen Concentration Distribution at End of Diffusion Analysis

5 Conclusion

This research demonstrated that both stress-assisted hydrogen diffusion and fatigue crack growth can be simulated in the finite element modeling software ABAQUS. The presented model is a proof of concept that should be further developed to couple the diffusion and fatigue simulations such that they occur in tandem (rather than in succession), to incorporate a traction separation law that allows for simulation of hydrogen induced decohesion, and to continuously modify the steel's mechanical properties to simulate the effects of hydrogen on plasticity near the crack tip, as was done in (10). This full simulation should then be calibrated to experimental data. A calibrated simulation can then be used for convenient, rapid predictions of crack growth rates in a variety of different hydrogen atmospheres and loading conditions. Such a simulation could also be used to quantify properties that are difficult to determine through experimentation and analytical methods, such as crack tip plasticity, and relate them to crack growth rate. Implementation of these relationships would have tremendous value in crack growth predictions in nontraditional operating conditions, such as overloading that results in significant crack tip plasticity (4).

Analysis of hydrogen-assisted FCG experiments was also performed as part of this work. The experimentation demonstrated the effects of varying loading frequency, hydrogen pressure, and steel microstructure on hydrogen assisted fatigue crack growth in steel, and can also be used in the future to calibrate a hydrogen assisted fatigue crack growth finite element model. In the beginning of the Paris regime of crack growth, crack growth rates were found to be faster in a 5000 psi H_2 environment than in an 800 psi H_2 environment, and faster in acicular ferrite steel than in ferrite pearlite steel. Toward the end of the Paris regime, the effects of hydrogen pressure and microstructure diminished, presumably because hydrogen could not diffuse through the steel fast enough to accelerate the rapidly advancing crack tip. Changes in frequency and microstructure did not affect crack growth rates in 5000 psi H_2,

possibly because the supply of hydrogen was so high at this pressure that the limiting steps in hydrogen assistance of crack growth rate were the reactions of hydrogen with the steel lattice, and not adsorption of hydrogen to the crack surfaces or transport of hydrogen to the crack tips. The extent to which hydrogen accelerates fatigue crack growth is thus clearly an intricate function of the magnitude of hydrogen supply, as is determined by the environing pressure and loading frequency, the rate of hydrogen diffusion to the crack tip, as is determined in part by the microstructure, and the rate of crack growth relative to the rates at which hydrogen enters the steel lattice and causes damage.

6 Bibliography

1. **Bannantine, Julie A., Comer, Jess J. and Handrock, James L.** *Fundamentals of Fatigue Analysis.* Englewood Cliffs : Prentice-Hall, Inc., 1990.

2. **Suresh.** *Fatigue of Materials.* New York : Cambridge University Press, 1998.

3. *Why K? High Order Singularities and Small Scale Yielding.* **Hui, C.Y. and Ruina, A.** 1995, International Journal of Fracture, Vol. 72, pp. 97-120.

4. **Janssen, M., Zuidema, J. and Wanhill, R.J.H.** *Fracture Mechanics.* Leeghwaterstraat, The Netherlands : VSSD, 2006.

5. *A micromechanics approach to the study of hydrogen transport and embrittlement.* **Taha, A. and Sofronis, P.** 2001, Engineering Fracture Mechanics, Vol. 68, pp. 803-837.

6. *Hydrogen effects on dislocaiton activity in austenitic stainless steel.* **Nibur, K.A., Bahr, D.F. and Somerday, B.P.** 2006, Acta Materialia, Vol. 54, pp. 2677-2684.

7. *Effects of alloy composition and strain hardening on tensile fracture of hydrogen-precharged type 316 stainless steels.* **San Marchi, C., et al., et al.** 2008, International Journal of Hydrogen Energy, Vol. 33, pp. 889-904.

8. *Grain Boundary Engineering Markedly Reduces Susceptibility to Intergranular Hydrogen Embrittlement in Metallic Materials.* **Bechtle, S., et al., et al.** 2009, Acta Materialia, Vol. 57, pp. 4148-4157.

9. *Effects of Gaseous Hydrogen on Fatigue Crack Growth in Pipeline Steel.* **Cialone, H.J. and Holbrook, J.H.** 1985, Metallurgic Transactions A, Vol. 16A, pp. 115-122.

10. *Toward a phenomenological description of hydrogen-induced decohesion at particle/matrix interfaces.* **Liang, Y. and Sofronis, P.** 2003, Journal of the Mechanics and Physics of Solids, Vol. 51, pp. 1509-1531.

11. *Hydrogen transport by dislocations.* **Tien, John, et al., et al.** 6, 1976, Metallurgical and Materials Transactions A, Vol. 7, pp. 821-829.

12. *Hydrogen-enhanced localized plasticity- a mechanism for hydrogen-related fracture.* **Birnbaum, H.K. and Sofronis, P.** 1994, Materials Science and Engineering, Vol. A176, pp. 191-202.

13. *The effect of hydrogen on dislocation dynamics.* **Robertson, I.M.** 2001, Vol. 68.

14. *Equilibrium aspects of hydrogen-induced cracking of steels.* **Oriani, R.A. and Josephic, P.H.** 9, 1976, Acta Metallurgica, Vol. 22, pp. 1065-1074.

15. *On a Surface Energy Mechanism for Stress Corrosion Cracking.* **Coleman, E.G., Weinstein, D. and Rostoker, W.** 5, 1961, Acta Metallurgica, Vol. 9, pp. 491-496.

16. *A brief history of fractography.* **Lynch, J.P. and Moutsos, S.** 6, 2006, Journal of Failure Analysis and Prevention, Vol. 6, pp. 54-69.

17. *Atomistic study of the effect of hydrogen on dislocation emission from a mode II crack tip in alpha iron.* **Taketomi, Shinya, Matsumoto, Ryosuke and Miyazaki, Noriyuki.** 2010, International Journal of Materials Science, Vol. 52, pp. 334-338.

18. *Hydrogen-enhanced dislocation activity and vacancy formation during nanoindentation of nickel.* **Wen, M., et al., et al.** 2009, Physical Review B., Vol. 80.

19. **Gangloff, R.P.** Hydrogen Assisted Cracking of High Strength Alloys. [ed.] I. Milne, et al., et al. *Comprehensive Structural Integrity.* New York : Elsevier Science, 2003.

20. *Hydrogen effects on the character of dislocations in high-purity aluminum.* **Ferreira, P.J., Robertson, I.M. and Birnbaum, H.K.** 10, 1999, Acta Materialia, Vol. 47, pp. 2991-2998.

21. **Reed-Hill, Robert E.** *Physical Metallurgy Principles.* 2. Boston : PWS-Kent Publishing Company, 1973.

22. *Influence of hydrogen coverage on the parameters of a cohesive zone model dedicated to fatigue crack propagation.* **Moriconi, C., Henaff, G. and Halm, D.** 2011, Engineering Procedia, Vol. 10, pp. 2657-2662.

23. *The effect of microstructure in the hydrogen embrittlement of a gas pipeline steel.* **Alp, T., Dogan, B. and Davies, T.** 1987, Journal of Materials Science, Vol. 22, pp. 2105-2112.

24. *Mechanistic dissimilarities between environmentally influenced fatigue-crack propagation at near-threshold and higher growth rates in lower strength steels.* **Suresh, S. and Ritchie, R.O.** 1982, Metal Science, Vol. 16, pp. 529-538.

25. *Multi-mechanism crack closure simulations in various steels.* **Castro, A. and Potirniche, G.P.** 2010, International Journal of Fatigue, Vol. 32, pp. 1764-1773.

26. *Hydrogen embrittlement in pre-deformed Ni3Al alloy.* **Li, Huaxin and Chaki, T.K.** 1995, Materials Science and Engineering A, Vol. 192/193, pp. 387-393.

27. *Hydrogen embrittlement susceptibility of a high-strength steel X80.* **Moro, I., et al., et al.** 2010, Materials Science and Engineering A, Vol. 527, pp. 7252-7260.

28. *Hydrogen Embrittlement of Metals.* **Louthan, M.R. Jr., et al., et al.** 1972, Materials Science and Engineering, Vol. 10, pp. 357-369.

29. *Influence of Hydrogen Pressure and Notch Severity on Hydrogen-environment Embrittlement at Ambient Temperatures.* **Walter, R.J. and Chandler, W.T.** 1971, Materials Science and Engineering, Vol. 8, pp. 90-97.

30. *Effects of hydrogen pressure and test frequency on fatigue crack growth properties of Ni-Cr-Mo steel candidate for a storage cylinder of a 70 MPa hydrogen filling station.* **Macadre, Arnaud, et al., et al.** 2011, Engineering Fracture Mechanics, Vol. 78, pp. 3196-3211.

31. *Effects of gaseous hydrogen and water vapor pressure on environmental embrittlement of Ni3Al.* **Lee, K.H., Lukowski, J.T. and White, C.L.** 1997, Intermetallics, Vol. 5, pp. 483-490.

32. *Brittle fracture in a ductile material with application to hydrogen embrittlement.* **Thomson, R.** 1978, Journal of Materials Science, Vol. 13, pp. 128-142.

33. *Hydrogen Embrittlement Mechanism in Fatigue of Austenitic Stainless Steels.* **Murakami, Yukitaka, et al., et al.** 2008, Metallurgical and Materials Transactions A, Vol. 39A, pp. 1327-1339.

34. *The Effect of Stress Ratio and Frequency on Fatigue Crack Growth.* **Musuva, J.K. and Radon, J.C.** 1979, Fatigue of Engineering Materials and Structures, Vol. 1, pp. 457-470.

35. *Recent progress in understanding environment assisted fatigue crack growth.* **Wei, R.P. and Simmons, G.W.** 2, 1981, International Journal of Fracture, Vol. 17, pp. 235-248.

36. *Hydrogen embrittlement of AISI 4130 steel with an alternate ferrite/pearlite banded structure.* **Lee, Huei-Long and Chan, Sammy Lap-Ip.** 1991, Materials Science and Engineering, A142, pp. 193-201.

37. *Effects of ferrite/pearlite alignment on the hydrogen permeation in a AISI 4130 steel.* **Tau, L. and Chan, S.L.I.** 1996, Materials Letters, Vol. 29, pp. 143-147.

38. *The Influence of Microstructure on Hydrogen Transport in Carbon Steels.* **Luu, W.C. and Wu, J.K.** 2, 1996, Corrosion Science, Vol. 38, pp. 239-245.

39. *The combined effect of frequency on load level on fatigue crack growth in stainless steel 304.* **Baik, Y.M. and Kim, K.S.** 2001, International Journal of Fatigue, Vol. 23, pp. 417-425.

40. **Hertzberg, Richard W.** *Deformation and Fracture Mechanics of Engineering Materials.* Fourth. Danvers : John Wiley & Sons, Inc., 1996.

41. *Effect of microstructure on the hydrogen trapping efficiency and hydrogen induced cracking of linepipe steel.* **Park, Gyu Tae, et al., et al.** 2008, Corrosion Science, Vol. 50, pp. 1865-1871.

42. *Hydrogen Cracking in Nominally Pearlitic 1045 Steel.* **Costa, James E. and Thompson, Anthony W.** 1982, Metallurgical Transactions A, Vol. 13A, pp. 1315-1318.

43. *Assessment of Pearlite Banding Using Automatic Image Analysis: Application to Hydrogen-Induced Cracking.* **Komenda, Jacek and Sandstrom, Rolf.** s.l. : 143-153, 1993, Materials Characterization, Vol. 31.

44. *Hydrogen transport near a blunting crack tip.* **Koers, R.W.J., Krom, A.H.M. and Bakker, A.** 1999, Journal of the Mechanics and Physics of Solids, Vol. 47, pp. 971-992.

45. *Numerical Analysis of Hydrogen Transport Near a Blunting Crack Tip.* **Sofronis, P. and McMeeking, R.M.** 1989, Journal of the Mechanics and Physics of Solids, Vol. 37, pp. 317-350.

46. *ABAQUS Online Documentation.* [Electronic] Providence : Dassault Systemes Simulia Corp., 2011.

47. *J-Integral Applied to Stress-Strain Concentrations.* **Szanto, M., Read, D.T.** 3, Boulder : s.n., 1992, Engineering Fracture Mechanics, Vol. 43, pp. 401-415.

48. *Prediction of the failure pressure for complex corrosion defects.* **Cronin, Duane S. and Pick, Roy J.** 2002, International Journal of Pressure Vessels and Piping, Vol. 79, pp. 279-287.

49. *The Influence of Crack-Face Fluid Pressure on the Fatigue Crack Propagation Due to Rolling Contact With Frictional Heat.* **Goshima, Takahito, Ishihara, Sotomi and Shimizu, Masayoshi.** 2002, Journal of Thermal Stresses, Vol. 25, pp. 373-388.

50. Kc of Materials. *efunda.* [Online] efunda. [Cited: 06 09, 2012.] http://www.efunda.com/formulae/solid_mechanics/fracture_mechanics/fm_lefm_Kc_Matl.cfm.

51. *Mode II Fracture Toughness of 4340 Steel.* **Tsangarakis, N.** 4, 1985, Engineering Fracture Mechanics, Vol. 22, pp. 617-624.

52. *Combined Mode I - Mode III Fracture Toughness of a High Carbon Steel.* **Manoharan, M., Hirth, J.P. and Rosenfield, A.R.** 1989, Scripta Metallurgica, Vol. 23, pp. 763-766.

53. *Guidelines and Parameter Selection for the Simulation of Progressive Delamination.* **Song, Kyongchan, Davila, Carlos G. and Rose, Cheryl A.** 2008. 2008 Abaqus Users' Conference. pp. 1-15.

54. **Group, Laser Analytics.** *Numerical Methods in Chemical Engineering.* s.l. : University of Cambridge, 2012.

55. *A direct method to predict cyclic steady states of elastoplastic structures.* **Spiliopoulos, Konstantinos V. and Panagiotou, Konstantinos D.** 2012, Computer Methods in Applied Mechanics and Engineering, Vols. 223-224, pp. 186-198.

56. **Fries, Thomas-Peter.** *The eXtended Finite Element Method.* [Electronic] Aachen, Germany : Computational Analysis of Technical Systems.

57. **McNary, Michael James.** Implementation of the Extended Finite Element Method (XFEM) in the ABAQUS Software Package. *Georgia Tech Theses and Dissertations.* [Online] 2009. [Cited: 6 10, 2012.] http://smartech.gatech.edu/jspui/handle/1853/29665?mode=full.

58. *A method for dynamic crack and shear band propagatin with phantom nodes.* **Song, Jeong-Hoon, Aerias, Pedro M. and Belytschko, Ted.** 2006, International Journal for Numerical Methods in Engineering, Vol. 67, pp. 868-893.

59. Specific Heat Metals. *Engineering ToolBox.* [Online] Engineering ToolBox. [Cited: 6 10, 2012.] http://www.engineeringtoolbox.com/specific-heat-metals-d_152.html.

60. Metal Alloy Densities. *Engineering ToolBox.* [Online] Engineering ToolBox. [Cited: 6 10, 2012.] http://www.engineeringtoolbox.com/metal-alloys-densities-d_50.html.

61. *The characteristics of hydrogen diffusion and concentration around a crack tip concerned with hydrogen embrittlement.* **Yokobori Jr., A. Toshimitsu, et al., et al.** 2002, Corrosion Science, Vol. 44, pp. 407-424.

62. *The Effect of Thickness on Hydrogen-Induced Slow Crack Growth.* **Gerberich, W.W. and Chen, Y.T.** 1974, Scripta Metallurgica, Vol. 8, pp. 243-248.

63. *The Role of Stress State on Hydrogen Cracking in Fe-Si Single Crystals.* **Chen, X., et al., et al.** 6, 1990, Engineering Fracture Mechanics, Vol. 35, pp. 997-1017.

64. *Effects of alloy composition and strain hardening on tensile fracture of hydrogen-precharged type 316 stainless steels.* **San Marchi, C., et al.** 2008, International Journal of Hydrogen Energy, Vol. 33, pp. 889-904.

65. *Near threshold fatigue crack growth in aluminum alloys at low and ultrasonic frequency: Influences of specimen thickness, strain rate, slip behaviour, and air humidity.* **Holper, B., et al., et al.** 2003, International Journal of Fatigue, Vol. 25, pp. 397-411.

7 Appendix A: ABAQUS Input File Code for Fatigue Crack Growth Simulation

Note: Code defining the nodes that comprise the part geometry has not been included.

```
*Heading
** Job name: 3dayfatigue Model name: Model-1
** Generated by: Abaqus/CAE 6.11-2
*Preprint, echo=NO, model=NO, history=NO, contact=NO
** ----------------------------------------------------------------
** PART INSTANCE: Specimen-1
** Section: Section-1
*Solid Section, elset=Specimen-1__PickedSet29, material=Material-1
*Surface, type=ELEMENT, name=_PickedSurf22
__PickedSurf22_S5, S5
*Enrichment, name=Crack-1, type=PROPAGATION CRACK, elset=_PickedSet24
*Amplitude, name=Amp-1, definition=PERIODIC
1,        6.28319,          0.,          3.
          0.,          1.
**
** MATERIALS
**
*Material, name=Material-1
*Damage Initiation, criterion=MAXPS
 3.509e+08,
*Damage Evolution, type=ENERGY, mixed mode behavior=BK, power=1.8
11271., 44380.,106348.
*Deformation Plasticity
 2.07e+11,       0.3, 3.509e+08,     8.072,     3.143
```

```
**
** INTERACTION PROPERTIES
**
*Surface Interaction, name=IntProp-1
1.,
*Surface Behavior
*Fracture Criterion, type=FATIGUE, mixed mode behavior=BK
 0.5, -1.44, 7.74412E-5, 2,,,11271.,44379.57333,106348.3256,    1.8
** PHYSICAL CONSTANTS
**
*Physical Constants, absolute zero=0., universal gas=8.314
*Initial Conditions, type=ENRICHMENT
341, 1,Crack-1, 0.000333334, 0.000932432
341, 2,Crack-1, 0.000333334, 0.000932432
341, 3,Crack-1, -0.000333333, 0.000932432
341, 4,Crack-1, -0.000333333, 0.000932432
341, 5,Crack-1, 0.000333333, -6.08102e-05
341, 6,Crack-1, 0.000333333, -6.08102e-05
341, 7,Crack-1, -0.000333333, -6.08101e-05
341, 8,Crack-1, -0.000333333, -6.08101e-05
342, 1,Crack-1, 0.000333334, 0.000932432
342, 2,Crack-1, 0.000333334, 0.000932432
342, 3,Crack-1, -0.000333333, 0.000932432
342, 4,Crack-1, -0.000333333, 0.000932432
342, 5,Crack-1, 0.000333333, -6.08102e-05
342, 6,Crack-1, 0.000333333, -6.08102e-05
342, 7,Crack-1, -0.000333333, -6.08101e-05
342, 8,Crack-1, -0.000333333, -6.08101e-05
```

343, 1,Crack-1, 0.000333334, 0.000932432

343, 2,Crack-1, 0.000333334, 0.000932432

343, 3,Crack-1, -0.000333333, 0.000932432

343, 4,Crack-1, -0.000333333, 0.000932432

343, 5,Crack-1, 0.000333333, -6.08102e-05

343, 6,Crack-1, 0.000333333, -6.08102e-05

343, 7,Crack-1, -0.000333333, -6.08101e-05

343, 8,Crack-1, -0.000333333, -6.08101e-05

344, 1,Crack-1, 0.000333334, 0.000932432

344, 2,Crack-1, 0.000333334, 0.000932432

344, 3,Crack-1, -0.000333333, 0.000932432

344, 4,Crack-1, -0.000333333, 0.000932432

344, 5,Crack-1, 0.000333333, -6.08102e-05

344, 6,Crack-1, 0.000333333, -6.08102e-05

344, 7,Crack-1, -0.000333333, -6.08101e-05

344, 8,Crack-1, -0.000333333, -6.08101e-05

305, 1,Crack-1, 0.000333333

305, 2,Crack-1, 0.000333333

305, 3,Crack-1, -0.000333333

305, 4,Crack-1, -0.000333333

305, 5,Crack-1, 0.000333333

305, 6,Crack-1, 0.000333333

305, 7,Crack-1, -0.000333333

305, 8,Crack-1, -0.000333333

306, 1,Crack-1, 0.000333333

306, 2,Crack-1, 0.000333333

306, 3,Crack-1, -0.000333333

306, 4,Crack-1, -0.000333333

306, 5,Crack-1, 0.000333333

306, 6,Crack-1, 0.000333333

306, 7,Crack-1, -0.000333333

306, 8,Crack-1, -0.000333333

307, 1,Crack-1, 0.000333333

307, 2,Crack-1, 0.000333333

307, 3,Crack-1, -0.000333333

307, 4,Crack-1, -0.000333333

307, 5,Crack-1, 0.000333333

307, 6,Crack-1, 0.000333333

307, 7,Crack-1, -0.000333333

307, 8,Crack-1, -0.000333333

308, 1,Crack-1, 0.000333333

308, 2,Crack-1, 0.000333333

308, 3,Crack-1, -0.000333333

308, 4,Crack-1, -0.000333333

308, 5,Crack-1, 0.000333333

308, 6,Crack-1, 0.000333333

308, 7,Crack-1, -0.000333333

308, 8,Crack-1, -0.000333333

269, 1,Crack-1, 0.000333333

269, 2,Crack-1, 0.000333333

269, 3,Crack-1, -0.000333333

269, 4,Crack-1, -0.000333333

269, 5,Crack-1, 0.000333333

269, 6,Crack-1, 0.000333333

269, 7,Crack-1, -0.000333333

269, 8,Crack-1, -0.000333333

270, 1,Crack-1, 0.000333333

270, 2,Crack-1, 0.000333333

270, 3,Crack-1, -0.000333333

270, 4,Crack-1, -0.000333333

270, 5,Crack-1, 0.000333333

270, 6,Crack-1, 0.000333333

270, 7,Crack-1, -0.000333333

270, 8,Crack-1, -0.000333333

271, 1,Crack-1, 0.000333333

271, 2,Crack-1, 0.000333333

271, 3,Crack-1, -0.000333333

271, 4,Crack-1, -0.000333333

271, 5,Crack-1, 0.000333333

271, 6,Crack-1, 0.000333333

271, 7,Crack-1, -0.000333333

271, 8,Crack-1, -0.000333333

272, 1,Crack-1, 0.000333333

272, 2,Crack-1, 0.000333333

272, 3,Crack-1, -0.000333333

272, 4,Crack-1, -0.000333333

272, 5,Crack-1, 0.000333333

272, 6,Crack-1, 0.000333333

272, 7,Crack-1, -0.000333333

272, 8,Crack-1, -0.000333333

233, 1,Crack-1, 0.000333333

233, 2,Crack-1, 0.000333333

233, 3,Crack-1, -0.000333333

233, 4,Crack-1, -0.000333333

233, 5,Crack-1, 0.000333333

233, 6,Crack-1, 0.000333333

233, 7,Crack-1, -0.000333333

233, 8,Crack-1, -0.000333333

234, 1,Crack-1, 0.000333333

234, 2,Crack-1, 0.000333333

234, 3,Crack-1, -0.000333333

234, 4,Crack-1, -0.000333333

234, 5,Crack-1, 0.000333333

234, 6,Crack-1, 0.000333333

234, 7,Crack-1, -0.000333333

234, 8,Crack-1, -0.000333333

235, 1,Crack-1, 0.000333333

235, 2,Crack-1, 0.000333333

235, 3,Crack-1, -0.000333333

235, 4,Crack-1, -0.000333333

235, 5,Crack-1, 0.000333333

235, 6,Crack-1, 0.000333333

235, 7,Crack-1, -0.000333333

235, 8,Crack-1, -0.000333333

236, 1,Crack-1, 0.000333333

236, 2,Crack-1, 0.000333333

236, 3,Crack-1, -0.000333333

236, 4,Crack-1, -0.000333333

236, 5,Crack-1, 0.000333333

236, 6,Crack-1, 0.000333333

236, 7,Crack-1, -0.000333333

236, 8,Crack-1, -0.000333333

197, 1,Crack-1, 0.000333333

197, 2,Crack-1, 0.000333333

197, 3,Crack-1, -0.000333333

197, 4,Crack-1, -0.000333333

197, 5,Crack-1, 0.000333333

197, 6,Crack-1, 0.000333333

197, 7,Crack-1, -0.000333333

197, 8,Crack-1, -0.000333333

198, 1,Crack-1, 0.000333333

198, 2,Crack-1, 0.000333333

198, 3,Crack-1, -0.000333333

198, 4,Crack-1, -0.000333333

198, 5,Crack-1, 0.000333333

198, 6,Crack-1, 0.000333333

198, 7,Crack-1, -0.000333333

198, 8,Crack-1, -0.000333333

199, 1,Crack-1, 0.000333333

199, 2,Crack-1, 0.000333333

199, 3,Crack-1, -0.000333333

199, 4,Crack-1, -0.000333333

199, 5,Crack-1, 0.000333333

199, 6,Crack-1, 0.000333333

199, 7,Crack-1, -0.000333333

199, 8,Crack-1, -0.000333333

200, 1,Crack-1, 0.000333333

200, 2,Crack-1, 0.000333333

200, 3,Crack-1, -0.000333333

200, 4,Crack-1, -0.000333333

200, 5,Crack-1, 0.000333333

200, 6,Crack-1, 0.000333333

200, 7,Crack-1, -0.000333333

200, 8,Crack-1, -0.000333333

161, 1,Crack-1, 0.000333333

161, 2,Crack-1, 0.000333333

161, 3,Crack-1, -0.000333333

161, 4,Crack-1, -0.000333333

161, 5,Crack-1, 0.000333333

161, 6,Crack-1, 0.000333333

161, 7,Crack-1, -0.000333333

161, 8,Crack-1, -0.000333333

162, 1,Crack-1, 0.000333333

162, 2,Crack-1, 0.000333333

162, 3,Crack-1, -0.000333333

162, 4,Crack-1, -0.000333333

162, 5,Crack-1, 0.000333333

162, 6,Crack-1, 0.000333333

162, 7,Crack-1, -0.000333333

162, 8,Crack-1, -0.000333333

163, 1,Crack-1, 0.000333333

163, 2,Crack-1, 0.000333333

163, 3,Crack-1, -0.000333333

163, 4,Crack-1, -0.000333333

163, 5,Crack-1, 0.000333333

163, 6,Crack-1, 0.000333333

163, 7,Crack-1, -0.000333333

163, 8,Crack-1, -0.000333333

164, 1,Crack-1, 0.000333333

164, 2,Crack-1, 0.000333333

164, 3,Crack-1, -0.000333333

164, 4,Crack-1, -0.000333333

164, 5,Crack-1, 0.000333333

164, 6,Crack-1, 0.000333333

164, 7,Crack-1, -0.000333333

164, 8,Crack-1, -0.000333333

125, 1,Crack-1, 0.000333333

125, 2,Crack-1, 0.000333333

125, 3,Crack-1, -0.000333333

125, 4,Crack-1, -0.000333333

125, 5,Crack-1, 0.000333333

125, 6,Crack-1, 0.000333333

125, 7,Crack-1, -0.000333333

125, 8,Crack-1, -0.000333333

126, 1,Crack-1, 0.000333333

126, 2,Crack-1, 0.000333333

126, 3,Crack-1, -0.000333333

126, 4,Crack-1, -0.000333333

126, 5,Crack-1, 0.000333333

126, 6,Crack-1, 0.000333333

126, 7,Crack-1, -0.000333333

126, 8,Crack-1, -0.000333333

127, 1,Crack-1, 0.000333333

127, 2,Crack-1, 0.000333333

127, 3,Crack-1, -0.000333333

127, 4,Crack-1, -0.000333333

127, 5,Crack-1, 0.000333333

127, 6,Crack-1, 0.000333333

127, 7,Crack-1, -0.000333333

127, 8,Crack-1, -0.000333333

128, 1,Crack-1, 0.000333333

128, 2,Crack-1, 0.000333333

128, 3,Crack-1, -0.000333333

128, 4,Crack-1, -0.000333333

128, 5,Crack-1, 0.000333333

128, 6,Crack-1, 0.000333333

128, 7,Crack-1, -0.000333333

128, 8,Crack-1, -0.000333333

89, 1,Crack-1, 0.000333333

89, 2,Crack-1, 0.000333333

89, 3,Crack-1, -0.000333333

89, 4,Crack-1, -0.000333333

89, 5,Crack-1, 0.000333333

89, 6,Crack-1, 0.000333333

89, 7,Crack-1, -0.000333333

89, 8,Crack-1, -0.000333333

90, 1,Crack-1, 0.000333333

90, 2,Crack-1, 0.000333333

90, 3,Crack-1, -0.000333333

90, 4,Crack-1, -0.000333333

90, 5,Crack-1, 0.000333333

90, 6,Crack-1, 0.000333333

90, 7,Crack-1, -0.000333333

90, 8,Crack-1, -0.000333333

91, 1,Crack-1, 0.000333333

91, 2,Crack-1, 0.000333333

91, 3,Crack-1, -0.000333333

91, 4,Crack-1, -0.000333333

91, 5,Crack-1, 0.000333333

91, 6,Crack-1, 0.000333333

91, 7,Crack-1, -0.000333333

91, 8,Crack-1, -0.000333333

92, 1,Crack-1, 0.000333333

92, 2,Crack-1, 0.000333333

92, 3,Crack-1, -0.000333333

92, 4,Crack-1, -0.000333333

92, 5,Crack-1, 0.000333333

92, 6,Crack-1, 0.000333333

92, 7,Crack-1, -0.000333333

92, 8,Crack-1, -0.000333333

53, 1,Crack-1, 0.000333333

53, 2,Crack-1, 0.000333333

53, 3,Crack-1, -0.000333333

53, 4,Crack-1, -0.000333333

53, 5,Crack-1, 0.000333333

53, 6,Crack-1, 0.000333333

53, 7,Crack-1, -0.000333333

53, 8,Crack-1, -0.000333333

54, 1,Crack-1, 0.000333333

54, 2,Crack-1, 0.000333333

54, 3,Crack-1, -0.000333333

54, 4,Crack-1, -0.000333333

54, 5,Crack-1, 0.000333333

54, 6,Crack-1, 0.000333333

54, 7,Crack-1, -0.000333333

54, 8,Crack-1, -0.000333333

55, 1,Crack-1, 0.000333333

55, 2,Crack-1, 0.000333333

55, 3,Crack-1, -0.000333333

55, 4,Crack-1, -0.000333333

55, 5,Crack-1, 0.000333333

55, 6,Crack-1, 0.000333333

55, 7,Crack-1, -0.000333333

55, 8,Crack-1, -0.000333333

56, 1,Crack-1, 0.000333333

56, 2,Crack-1, 0.000333333

56, 3,Crack-1, -0.000333333

56, 4,Crack-1, -0.000333333

56, 5,Crack-1, 0.000333333

56, 6,Crack-1, 0.000333333

56, 7,Crack-1, -0.000333333

56, 8,Crack-1, -0.000333333

17, 1,Crack-1, 0.000333333

17, 2,Crack-1, 0.000333333

17, 3,Crack-1, -0.000333333

17, 4,Crack-1, -0.000333333

17, 5,Crack-1, 0.000333333

17, 6,Crack-1, 0.000333333

17, 7,Crack-1, -0.000333333

17, 8,Crack-1, -0.000333333

18, 1,Crack-1, 0.000333333

18, 2,Crack-1, 0.000333333

18, 3,Crack-1, -0.000333333

18, 4,Crack-1, -0.000333333

18, 5,Crack-1, 0.000333333

18, 6,Crack-1, 0.000333333

18, 7,Crack-1, -0.000333333

18, 8,Crack-1, -0.000333333

19, 1,Crack-1, 0.000333333

19, 2,Crack-1, 0.000333333

19, 3,Crack-1, -0.000333333

19, 4,Crack-1, -0.000333333

19, 5,Crack-1, 0.000333333

19, 6,Crack-1, 0.000333333

19, 7,Crack-1, -0.000333333

19, 8,Crack-1, -0.000333333

20, 1,Crack-1, 0.000333333

20, 2,Crack-1, 0.000333333

20, 3,Crack-1, -0.000333333

20, 4,Crack-1, -0.000333333

20, 5,Crack-1, 0.000333333

20, 6,Crack-1, 0.000333333

20, 7,Crack-1, -0.000333333

20, 8,Crack-1, -0.000333333

**

** BOUNDARY CONDITIONS

**

** Name: BC-1 Type: Displacement/Rotation

```
*Boundary
_PickedSet18, 3, 3
_PickedSet18, 4, 4
_PickedSet18, 5, 5
** ----------------------------------------------------------------
**
** STEP: Step-2
**
*Step, name=Step-2, inc=100000
*Direct Cyclic, continue=YES, fatigue, cetol=0.001
259200., 259200, 0.1, 259200., , , , 999
**
** LOADS
**
** Name: Load-1   Type: Pressure
*Dsload, amplitude=Amp-1
_PickedSurf22, P, -1.700680272e+07
**
** OUTPUT REQUESTS
**
*Restart, write, frequency=0
**
** FIELD OUTPUT: F-Output-1
**
*Output, field
*Node Output
CF, PHILSM, PSILSM, RF, RM, RT, TF, U
UR, UT, VF
```

*Element Output, directions=YES

ALPHA, ALPHAN, BF, CENTMAG, CENTRIFMAG, CFAILURE, CORIOMAG, CS11, CTSHR, DAMAGEC, DAMAGET, ESF1, GRAV, HP, JK, MISES

MISESONLY, NFORC, NFORCSO, P, PE, PRESSONLY, PS, ROTAMAG, S, SDEG, SF, SSAVG, TRNOR, TRSHR, TSHR, VS

PEEQ

*Contact Output

BDSTAT, CRSTS, CSDMG, DBS, DBSF, DBT, EFENRRTR, ENRRT, OPENBC

**

** HISTORY OUTPUT: H-Output-1

**

*Output, history, variable=ALL

*EL FILE, POSITION=AVERAGED AT NODES

SINV,

*End Step

8 Appendix B: ABAQUS Input File Code for Stress-Driven Hydrogen Diffusion Simulation

Note: Code defining the nodes that comprise the part geometry has not been included

```
*Heading
** Job name: Diffusion Model name: Model-1
** Generated by: Abaqus/CAE 6.11-2
*Preprint, echo=NO, model=NO, history=NO, contact=NO
** ----------------------------------------------------------------
**
** Section: Section-1
*Solid Section, elset=Specimen-1__PickedSet29, material=Material-1
,
*System
*Nset, nset=_PickedSet25, generate
  1,  7600,    1
*Elset, elset=_PickedSet25, generate
  1,  5772,    1
*Nset, nset=_PickedSet26, generate
  1,  7600,    1
*Elset, elset=_PickedSet26, generate
  1,  5772,    1
** MATERIALS
**
*Material, name=Material-1
*Density
7850.,
*Diffusivity, law=FICK
```

7.272e-11,1000.

*Kappa, type=PRESS

1.64636e-06, 0.754

*Solubility

0.0003209,

*Specific Heat

490.,

**

** PHYSICAL CONSTANTS

**

*Physical Constants, absolute zero=0., universal gas=8.314

**

** BOUNDARY CONDITIONS

**

** Name: BC-1 Type: Displacement/Rotation

*Boundary

_PickedSet25, 3, 3

_PickedSet25, 4, 4

_PickedSet25, 5, 5

**

** PREDEFINED FIELDS

**

** Name: Predefined Field-1 Type: Temperature

*Initial Conditions, type=TEMPERATURE

_PickedSet26, 343.15

** Name: Predefined Field-2 Type: Temperature

*Initial Conditions, type=CONC

_PickedSet27, .75355

```
** ----------------------------------------------------------------
**
** STEP: Step-1
**
*Step, name=Step-1
*Mass Diffusion, steady state
1., 1., 1e-05, 1.,
*PRESSURE STRESS,FILE= 3dayfatigue
**
** OUTPUT REQUESTS
**
*Restart, write, frequency=0
**
** FIELD OUTPUT: F-Output-1
**
*Output, field, variable=PRESELECT
**
** HISTORY OUTPUT: H-Output-1
**
*Output, history, variable=PRESELECT
*End Step
```